Mahatma Education Society's

Pillai HOC College of Arts, Science and Commerce

Pillai HOCL Educational Campus, Rasayani

NAAC Accredited with A+ Grade in Cycle 2

(ISO 9001: 2015 Certified)

3.3.2. QnM.

Number of research papers per teachers in the Journals notified on UGC website

(A.Y. 2022-23)

PILLAI HOC COLLEGE OF ARTS, SCIENCE & COMMERCE * RASAYANI *

PRINCIPAL
Mahatma Education Society's
Pillai HOC College of
Arts, Science & Commerce
Pillai HOC Educational Campus
Rasayani Taluka Khalapur
Dist. Raigad, Pin- 410 207

Atmospheric Sciences

First Results From Imaging Riomter Installed At Indian Antarctic Station Maitri, Antarctica

Jayanta K. Behera[1], A. K. Sinha[1], Ajay Dhar[1], B. M. Pathan[1], K. U. Nair[1],C. Selvaraj[1] and P. Elang[2], and K. Jeeva[2]

[1]Indian Institute of Geomagnetism, New Panvel (W), Navi Mumbai 410 218, India.

[2]Equatorial Geophyscal Research Laboratory, VittalapuramVilakku, Krishnapuram, Maharajanagar, Tirunelveli 627 011, India.

Abstract:

An imaging Riometer has been installed at Indian Antarctic station Maitri (Geographic 70.75 degree S, 11.75 degree E; corrected geomagnetic 63.11 degree S, 53.59 degree E) in February 2010. This paper presents some of the salient results obtained during the year 2011 in 30 Indian Scientific Expedition to Antarctica.

Sidereal shift of around 2 hours in the diurnal pattern validates the data obtained from the newly installed instrument. Moreover, the strength of cosmic noise signal on quiet days also varies with months. This is apparently due to solar ionization of D-region ionosphere causing enhanced electron density where collision frequency is already high. The main objective of installing the imaging Riometer at Maitri is to study magneotspheric-ionospheric coupling during substorm processes. In the current study, we present two typical examples of disturbed time CNA associated with storm-time and non-storm time substorm. Results reveal that CNA is more pronounced during storm-time substorm as compared to non-storm time substorm. The level of CNA strongly depends upon the strengthening of convectional electric field and the duration of south-ward turning of interplanetary magnetic field before the substorm onset.

Keywords: *imaging Riometer, CNA, Magnetospheric substorm, Geomagnetic storm, Auroral electrojet.*

1. Introduction:

Studies of ionospheric absorption of radio waves are thus of considerable interest to the communication engineers and space researchers. So requirement of an instrument to monitor the lower ionosphere is unavoidable. Earlier wide beam Riometer has been used for this purpose since 1950s. Basically, Riometer is the acronym of Relative Ionospheric Opacity Meter using Extra Terrestrial Electromagnetic Radiation. It is an important ionospheric diagnostic tool which uses

the randomly fluctuating, almost 'white', noise from galactic radio sources as probing signals to investigate the upper, ionized part of the Earth's atmosphere [Little, 1954; Little and Leinbach, 1958, 1959]. Outside the influence of the Earth's environment these radio signals have fairly constant intensities [Stauning, 1984]. Absorption of the cosmic radio signal is experienced due the ionosphere at frequencies above 15 MHz when highly directional antennas are pointed towards the particular part of the sky. Celestial objects like Quasars, super dense objects that lie far from Earth, emit electromagnetic waves in its entire spectrum including radio waves.

1.1 Indian perspective of Ionospheric study using Cosmic Noise study:

Indian contribution to the study of cosmic noise started six decades ago. Mitra and Shain [1953] introduced cosmic noise method for the first time. The ionospheric absorption was measured by comparing the signal strength of extraterrestrial radio waves received on a fixed receiving system with the signal strength received on the same system at the same sidereal time under conditions of negligible ionospheric absorption. Bhonsle and Ramanathan [1958] reported absorption in the D-region over Ahmedabad, India (geographic: 23.02 degree N, 72.38 degree E) by using riometer at 25 MHz. Occurrence characteristic of ionospheric absorption in the time period from afternoon to evening is consistent with the daily variation of the ionospheric F- region absorption associated with increases of foF2 which were obtained from the statistical analysis of the riometer absorption on 25 MHz at Ahmedabad in India [Abdu et al., 1967]. Diurnal and seasonal variation of total ionospheric absorption (L) at an equatorial station, Trivandrum (dip 0.6 S, geographic long 76.56 degree E) has been studied using two years riometer data [Parameshwan et al.,1976]. They have investigated the dependence of L on geophysical parameters and sunspot numbers. In addition to that, they have estimated the electron tempearature of F-region from the F-region contribution to the total absorption. Lunetta and Abdu [1971] suggested that the absorption of cosmic radio noise varies with the latitude of the observations.

2 Technique for deriving QDC:

The method of determining QDC of cosmic noise signal has been discussed extensively by several authors [e.g., Mitra and Shain, 1953; Lusignan, 1960; Steiger and Warmick, 1967; Armstrong et al. 1977; Krishnaswamy et al.,1985; Tanaka et al., 2007, etc]. Recently, Moro et al, [2012] have presented new modified technique for Riometer Network (SARINET) data from South America with respect to method of Tanaka et al., [2007]. In that paper, two criteria have been followed: (1) Riometer data selection according to the geomagnetic activity and (2) data cleaning with respect to electromagnetic interference as well as some other noises.

In the current approach for deriving QDC of cosmic noise signal, we have used two criteria as followed by Moro et al.[2012]. For fulfillment of the first criteria, the

average of imaging Riometer data for the five international quietest days was used to derive QDC for a particular month. Table 1 is showing the list of days taken in a month during the year 2010-2011 for deriving QDC. It should be noted that only 6 days data were available during December,2010, out of that only one day was magnetically quiet(K_p < 3). The second criteria are taken for removing electromagnetic interference. This may be produced due to presence of man-made interference, thunderstorms or solar noise bursts. These bursts can affect the estimation of the QDC leading to an increase of the QDC level. [Moro et al, 2012]. Here, we have taken the selected days for the year 2010 and 2011 confining to quietest days of month. The error limit of QDC curve ranges from 0.02 dB to 0.30 dB. The maximum error value has been recorded in January month and minimum in the September month. Since imaging Riometer can serve both the narrow beam application as well as wide beam application, we have chosen the solar zenith corrected wide beam data for this study. The imaging riometer data set has inbuilt provision to differentiate wide beams and narrow beams. In figure (1), QDC of each month have been plotted.

Table:1 List of number of quiet days considered for QDC analysis of cosmic noise signal. Conitunes 12 months period of imaging Riometer data have been taken from November,2010 to October, 2011. This period is taken as per the data availability and quality.

Year	**Months**	**No. of days**
2010	November	04
	December	01
2011	January	04
	February	05
	March	05
	April	05
	May	05
	June	05
	July	04
	August	05
	September	05
	October	05

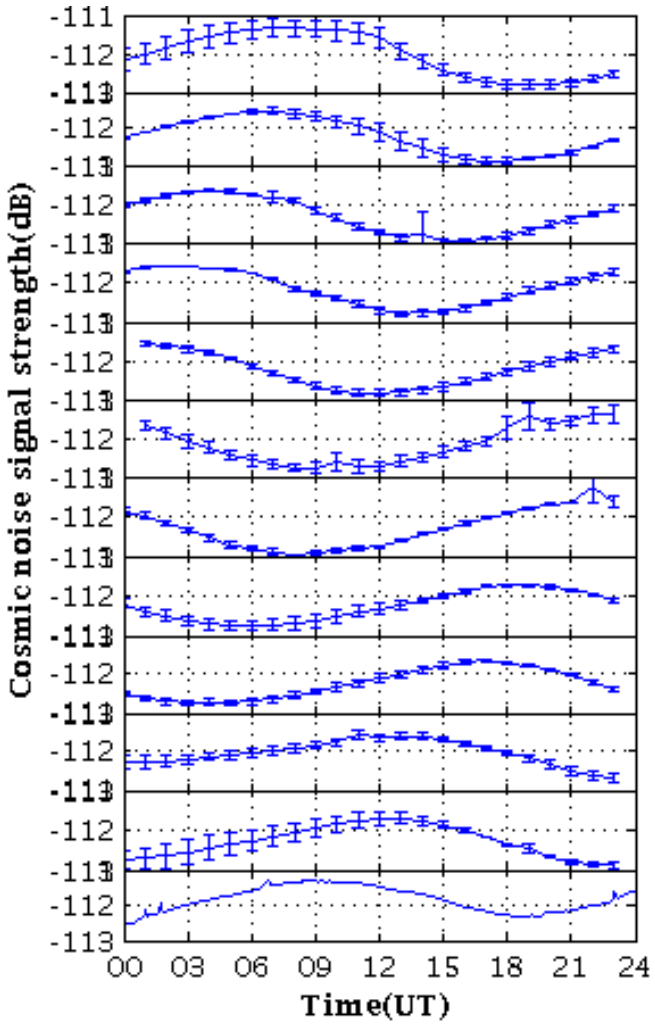

Figure 1. Quiet Day Cosmic noise signals or, Quiet day curves(QDCs) for each months of year 2010-11.Here wide beam(beam 17) data of imaging Riometer was used for deriving QDCs.

2.1Sidereal time and Monthly variation of QDC at Maitri, Antarctica:

The signal strength of radio noises, coming from the inter-stellar space varies with sidereal time (time scale based on earth's rate of rotation measured relatively to fixed stars) and months. In general, average sidereal day is of 23 hr 56 min and 4 seconds where as the solar day is of 24 hrs. So there is an approximately 4 minute difference between sidereal and solar day. Imaging Riometer data is in solar time format. While deriving QDC, with respect to solar time, we would expect a shift of about 2 hr (30days X 4 min) in the diurnal pattern of signal strength between consecutive months. This seems to be a genuine tool to assess the accuracy as well as the correctness of data and thereby validating the new dataset.

We observed an approximate shift of around 2 hr in the consecutive months that can be seen in figure (3). In January, the maximum value of the signal strength has been

obtained at around 0900 UT, whereas in February month, the occurrence time of maximum value has shifted around 0700 UT. Similarly for other months, the shift of 2 hrs is consistently observed. Moreover, if one follows the red tone which represents the maximum strength of QDC, around 2 hr/month shift is consistently observed.

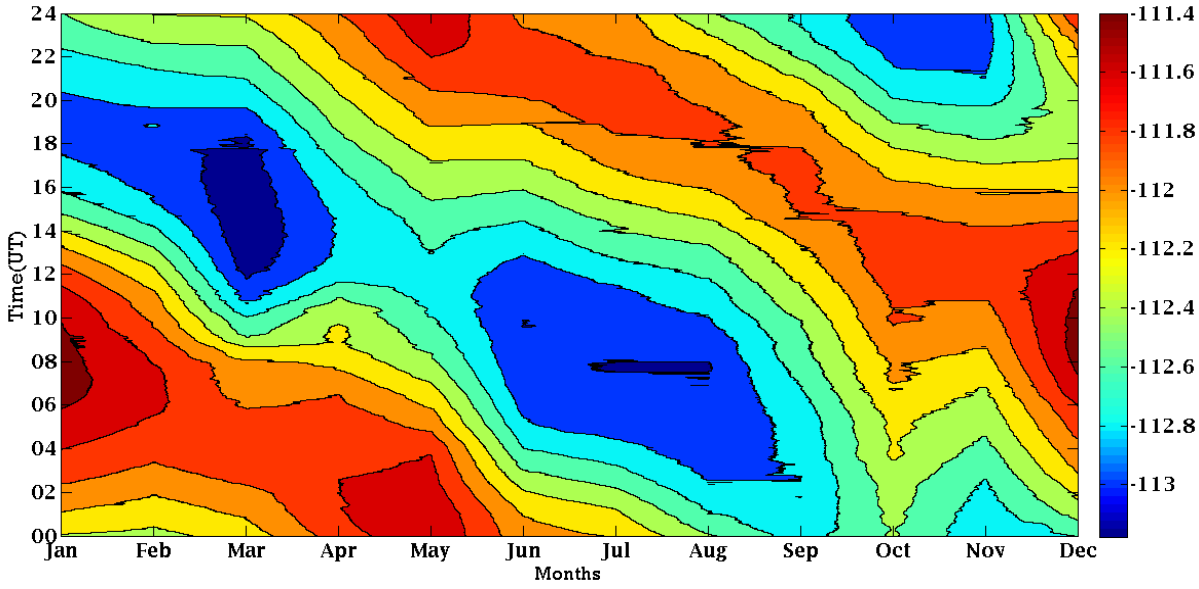

Figure 2. Contour plot for Sidereal shift of maximum signal strength of Cosmic noise signal for consecutive months. For the month January to May, shift of ~ 10 hours (~ 10 UT to 00 UT) of maximum signal strength is seen. Similarly, for the month June to December, shift of ~14 hours (~24 UT to 10 UT) is seen.

In quiet conditions of ionosphere over the station of Maitri, cosmic noise signal has a regular diurnal pattern (figures (2) and (3)). However, sun can also influence the level of signal through following mechanism. The ultraviolet rays of the sun enhances the ionization of the ionosphere which ultimately causes more absorption of signal of cosmic noises even in a quiet day, when there is no additional input of particle flux from the magnetosphere, e.g., during substorm phenomena [Browne et al., 1995]. At Antarctica, seasonal variation of strength of quiet day curves of cosmic noises has been observed. Figure (3) shows a seasonal variation of the cosmic noise signal strength. In three panels, average strength, maximum strength and minimum strength of the QDC of cosmic noise signal for each month have been plotted respectively. There is comparatively maximum drop of signal strength (average, maximum and minimum) in the month of March (autumn equinox month) and August (pre-spring equinox month). However, the average strength of cosmic noise signal is maximum (~ -112.03 dB) in the month of May, which is in winter season and (~ -111.95 dB) in December month in summer at Antarctica. From Equation (1), one would expect higher cosmic noise signal strength during winter (no-Sun) months when ionospheric conductivity is less and opposite for summer (sunlit) months.

However, in our observation, we see very complex behavior of signal strength variation over months (Figure 4). When austral winter approaches (March onwards) signal strength rises (as expected), whereas for the rest of the months variations are quite random. For example, sudden drop in signal strength from January to March (summer season), May to June (winter in progress) and relatively constant variation till the commencement of austral summer and further increase cannot be explained on the basis of solar illumination. It makes us to believe that other factors significantly contribute towards the seasonal variation of signal strength of QDC.

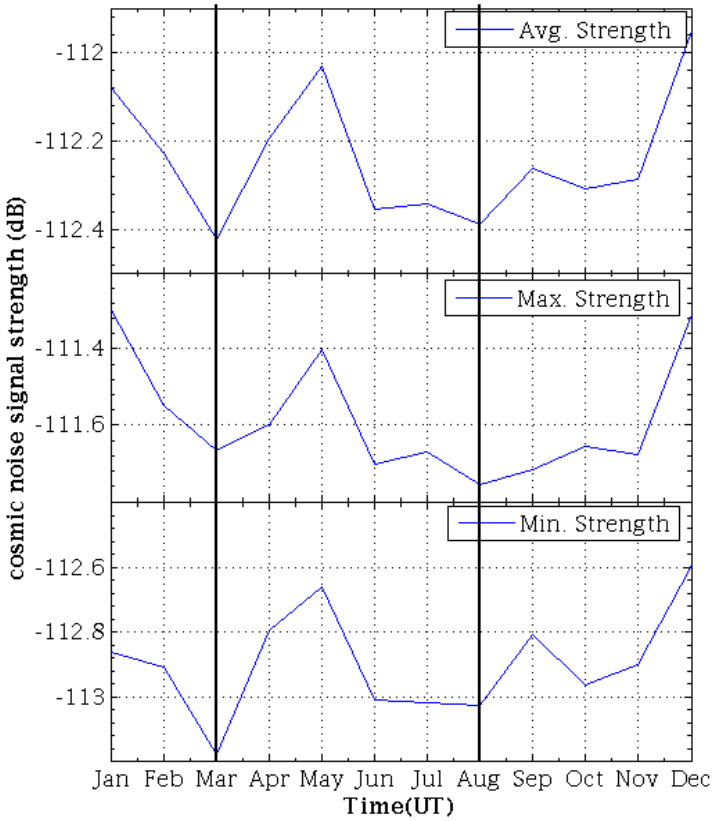

Figure 3. *Seasonal variation of cosmic noise signal strength: Upper, middle and lower panels are respectively for average, maximum and minimum strength value.*

3. Observations of CNA during storm-time and non-storm time substorms:

In the present study, we have examined CNA characteristics during storm time substorm and non-storm substorm occurring near midnight hours at Maitri on 12 April 2011 and 09 July 2011 respectively. We observe that Maitri comes under the influence of westward electrojet for both the events. However, there is a subtle difference to note between these two events.

12 April 2011* Event *of CNA during the storm time substorm:

Cosmic noise absorption (CNA), in association with the magnetospheric substorm occurred during 0600-0800 UT on 12 April 2011 has been shown. For this event Maitri station would lie in 0500-0700 MLT interval as MLT = UT-1 for our station. In figure (4), we depict the interplanetary magnetic field (IMF) and solar wind velocity as observed by instruments aboard ACE satellite located outside of the Earth's magnetosphere (at X = 229.6 *Re*, Y = - 21.5 *Re*, Z = - 40.9 *Re* in GSM coordinate system: here Re is the radius of the earth ~ 6378 km). In order to corroborate the interplanetary observations with ground magnetic data, IMF and solar wind data have been delayed by 60 minutes taking into account the travel time of solar wind at an average speed of ~ 500 km/s from the location of the satellite to the magnetopause of the earth. The upper first two panels represent the IMF Bz and solar wind velocity (Vs) respectively. In the next two panels, SYM-H and AL-index have been plotted respectively. The bottom four panels represent the H-component of geomagnetic field, cosmic noise signals, relative CNA and image of CNA over Maitri station. In the sixth panel, quiet day signal of April month and signal of individual day (12 April 2011) has been plotted. We obtained CNA (the bottom most panel) for the day by taking difference of cosmic noise signal of that day in a month from the QDC of the same month. The bottom most panel shows the image plot of CNA during the event. It has been observed that CNA become more intense during the period of 0630-0730 UT.

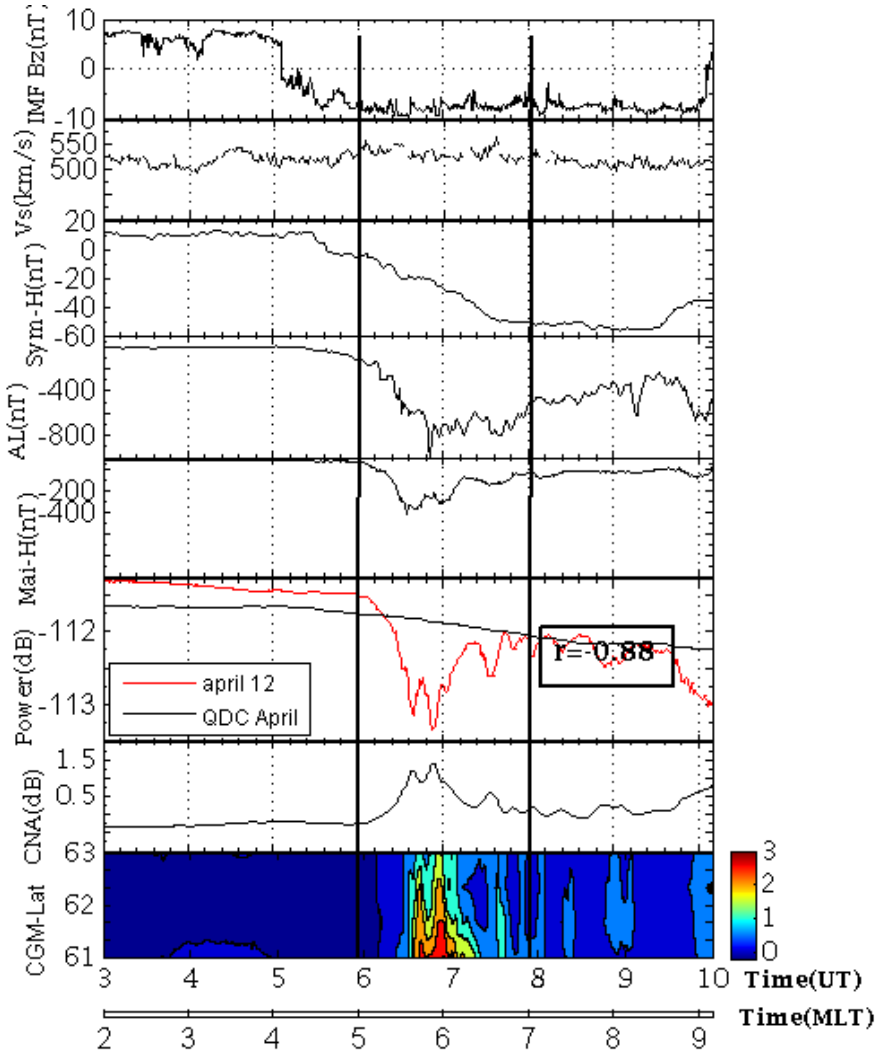

Figure 4. *(form top to bottom) Bz component of interplanetary magnetic field (IMF) , solar wind velocity (Vs) as observed by ACE satellite, Sym-H index , AL index, geomagnetic H-component variation, cosmic noise signal power(red line indicates the signal strength of 12 April 2011, where as the black line indicates the quiet day signal for the April month), CNA and image of CNA at Maitri station. Interplanetary observations are delayed by 60 min to compare with the gorund data. This event represents the CNA during storm time-substorm. Correlation coeffiecient between H-componet and CNA in this case is high (r= -0.88).*

The onset of substorm can be clearly seen at ~ 0600 UT in the AL-index with a sharp depression of ~1000 nT (figure 5). This appears to be a storm time substorm event as the SYM-H index value has gone down to -50 nT [Hsu et al, 1998). The solar wind velocity on that particular day was high (~ 500km/sec) and steadily increased up to 550 km/sec. The solar wind velocity was steady during all the phases of substorm. The Substorm triggering initiated with sharp southward turn of IMF Bz at ~ 0500 UT. It remained southward for 5 hrs then turned northward at 1010 UT approximately. At the onset of substorm, simultaneous occurrence of westward electrojet and cosmic noise absorption (CNA) has been observed over Matri. Intensity of the westward electrojet is weaker over Maitri (H depression ~-350 nT) than what is observed in the AL index. This could be due to the fact that Maitri station was around 0500 hr MLT and quite away from the center of the westward electrojet which peaks around midnight [Allen and Kroehl, 1975; Singh et al., 2012]. Moreover, due to the absorption of cosmic radio signal, it was attenuated by more than 1.5 dB in comparison to monthly QDC (see bottom panel of Figure 5). It should be noted that the correlation coefficient (r) between H-component and strength of CNA during the event (0500-0700 MLT) at Maitri for this event is very high (r= -0.88).

09 July 2011 event of CNA during non-storm time substorm event:

On 09 July 2011, we observed a substorm during 0300-0500 UT which is not accompanied by storm. For this event, Maitri station would be in the post-midnight hour (0200-0400 MLT). Top two panels of figure (5) depict the IMF Bz and solar wind velocity (Vs) as observed by instruments aboard ACE satellite. During this event the location of ACE was at X = 237.9 *Re*, Y = 40.4 *Re*, Z = 23.0 *Re* in GSM coordinate system. In order to relate the interplanetary observations with ground magnetic data, IMF and solar wind data have been delayed by 71 minutes taking into account the travel time of solar wind at an average speed of ~ 340 km/s from the location of the satellite to the magnetopause of the earth. In the next two panels, SYM-H and AL index have been plotted respectively. The bottom four panels respectively show H-component of geomagnetic field, Cosmic noise signals, relative CNA and image of CNA respectively at Maitri. In the sixth panel, quiet day signal of July month and signal of 09 July 2011 has been plotted. We obtained CNA (the bottom most panel panel) for the day by taking difference of cosmic noise signal of that day in a month from the QDC of the same month. The bottom most panel shows the image plot of CNA during the event. It has been observed that CNA become relatively stronger during a small period of 0340-04310 UT.

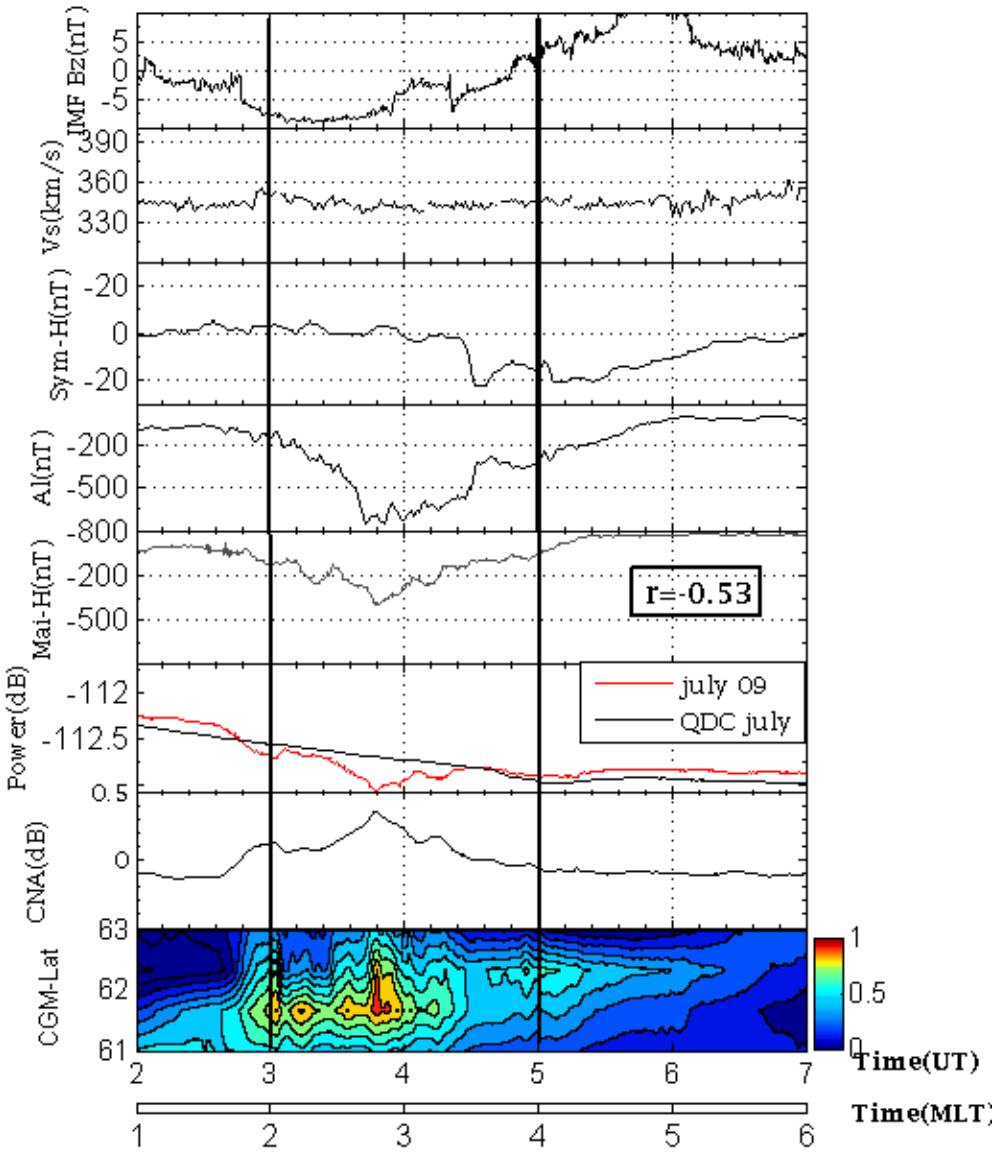

Figure 5. *(form top to bottom) Bz component of interplanetary magnetic field (IMF) , solar wind velocity (Vs) as observed by ACE satellite, Sym-H index , AL index, geomagnetic H-component variation and cosmic noise signal power (red line indicates the signal strength of 09 July 2011, where as the black line indicates the quiet day signal for the July month), CNA and image of CNA at Maitri station. Interplanetary observations are delayed by 71 min to compare with the gorund data. This event represents the CNA during non-storm time substorm. Correlation coeffiecient between H-componet and strength of CNA in this case is less (r= -0.53).*

Generally, non-storm time substorms have no sign of simultaneous storm [Hsu et al, 1998]. At the time of onset (~ 0300 UT) of substorm the sym-H index was ~ 1 nT, which clearly shows no signature of enhancement of ring currents. The magnitude of

AL-index was ~700 nT. Simultaneous observation of solar wind velocity for ACE satellite showed steady and slow flow of solar wind having velocity ~340 km/s with southward IMF Bz. This non storm time substorm led to a less amount of absorption of cosmic noise (~0. 4 dB) along with almost same magnitude of westward electrojet (-350 nT) despite the fact that AL-index was less (~700 nT) as compared to storm-time substorm of 12 April 2011 seen over Matri station. This is for the reason that Maitri was at around 0200 hr MLT and relatively nearer to the centre of westward electrojet (discussed earlier in the figure 5). The correlation coefficient between H-component and strength of CNA during the event (0200-0400 MLT) at Maitri in this case was found to be less (r= -0.53) as compared to storm-time substorm case of 12 April 2011. However, we obtained better (r= -0.75) when we restrict the calculation of correlation coefficient within the time limit (0200-0330 MLT). This time limit has been taken due to the fact that CNA lasts for this period of time only during the event.

4. *Discussion* and Conclusion:

For the first time, data of imaging Riometer at Maitri, Antarctica have been used to study the substorm activity at Maitri in this work. The observation of CNA using Imaging Riometer could be a great asset for carrying out the research in sub-auroral ionosphere. The usefulness of this instrument is remarkable in understanding of precipitation dynamics due to substorm processes at sub-auroral latitude region. In this paper we have given a brief account of the background, theory and instrumentation with an emphasis on validating the newly obtained data set.

The quiet day curve (QDC) of any new instrument is most essential part of study. One has to understand the daily and seasonal variation of QDC of new instrument for further research. So, here we have discussed about the sidereal and monthly variation of QDCs. A consistent sidereal shift of ~2hrs in each consecutive month has been seen which signify the consistency and reliability of the new instrument. Thus, the shifting of the main source of the cosmic noise signal with sidereal time can be clearly identified.

Monthly variation of cosmic noise signal in quiet condition i.e QDCs not only depends on the source of galactic cosmic noise but also on other factors. It seems other things such as orbital motion of the earth, the distance of the sun from the earth and level of ionization in the D-region during various months, responsible for cosmic noise during various months have simultaneous impact on the cosmic noise signal variation with months.

And finally, we have shown two different cases of CNA during storm time and non-storm time substorms, both occurring in post midnight to early morning sector. Magnetic reconnection [e.g., Baker et al., 1996] and dipolarization/current disruption e.g. [Lui, 1998] in the near-earth magnetotail have been suggested as the cause of substorm expansion onsets. Initially it was suggested that storm and nonstorm time substorms are manifestation of different mechanism, namely magnetic reconnection

and current disruption respectively [Baumjohan et al., 1996]. But later it was shown that storm and non-storm time substorms do not differ qualitatively in the generation mechanism [Hsu and McPherron, 1998]. Nevertheless, the energy accumulation and the dipolarization tend to be more significant during storm time substorms.

Maitri is a sub-auroral station located in Antarctica and it is expected that the auroral oval would expand and cover Maitri location during disturbed days. Hence the station will come under the influence of Auroral electrojet. Here, during both the CNA events associated with magnetospheric substorm, the equatorward expansion of auroral oval has taken place. In case of CNA event occurring 12 April 2011 during storm-time substorm, the auroral electrojet was slightly stronger (AL ~ 1000 nT] as compared with the non-storm time substorm event of 09 July 2011 (AL ~ 700 nT). During both the substorms, clear influence of west ward electrojet of almost the same magnitude (~ 350 nT) with simultaneous occurrence of CNA was observed over Matri. Maitri was nearer to the onset location of substorm of later case (09 July 2011- non-storm time) compared to that during 12 April 2011- storm-time, as the MLT range for the event on 09 July 2011 was 02-04 hrs and it was 05-07 hrs for 12 April 2011. There are different kinds of CNA event depending on the local time and magnetospheric phenomena [stauning, 1994]. However the above two CNA events which have examined in this study, are confirmed to be associated with substorms. This kind of absorption is due to the precipitation of energetic electrons (energy range from 10 to 100 KeV) in the E- region and upper D-region (~ 70-100 km) [Kellerman, 2009].

While comparing the two events, we observed higher CNA for the storm-time substorm event. During storm-time substorm, the south-ward turning of IMF Bz occurred at around 0500 UT and was sustained up to 6 hrs. Moreover, the solar wind velocity (**v**) was high (~550 km.) during the event. Thereby the convection electric field (- **V** X **Bz**) was stronger (5.5 mV/m.) and was sustained for longer period of time (~6 hrs) which we can infer from the figure 5. One thing should be noticed in this storm-time substorm event is the difference of ~01 hr between the south-ward turning of IMF Bz and onset of substorm. That means strengthening of convection electric field occurred much earlier (~ 01 hr) that drove more flux of energetic charge particles in to the magnetosphere and caused subsequent loading of particles in to the magneto-tail region before the re-connection occur. Whereas, the other event of non-storm time substorm (figure 6) clearly shows weaker convection electric field (~3.4 mV/m.) for lesser period of time (~ 2 hrs). During this event the southward turning of IMF Bz occurred only 10 minutes before the onset of substorm and was sustained for comparatively less time (~ 2 hr.) as compared to the storm-time substorm event. In addition to that, the solar wind velocity (**V**) was also moderate (~340 km.) during this event. This clarifies that level of CNA is more related to loading of the particles and intensity of reconnection in the magnetotail. These results also strongly support the difference between storm-time substorm and non-storm time substorm characteristics stated by Hsu and McPherron [1998]. They clearly mentioned in their paper in 1998 that the energy accumulation and the

dipolarization tend to be more significant during storm time substorms. Moreover, the reconnection of higher intensity also triggered a moderate storm which was associated with the 12 April 2011 event.

Finally, we can conclude that depression in geomagnetic H-component and CNA at Maitri are the consequences of flux of electrons intensifying the auroral electrojet and precipitation of electrons enhancing the conductivity of the upper D-region respectively. The correlation coefficient between H-component and CNA strength at Maitri is -0.88 for storm time substorm event and it is -0.53 for non-storm time substorm event. Correlation co-efficient for both the events are significant as enough number of data points (~ 7200) have gone in to the analysis. It is clear that CNA and H-component of geomagnetic field variation correlate well for both the events. However the extent of CNA depends on the strength of the magnetospheric convection electric field and the duration of southward IMF Bz before the substorm onset. Nevertheless, a proper statistical study may explore the possible empirical relationship between convection electric field and CNA at a sub-auroral station such as Maitri.

Acknowledgement:

The authors are indebted to F. Honary and group from Lancaster University for their invaluable help in installing of imaging Riometer and preliminary data processing. The authors express their sincere thanks to National Centre for Antarctic & Ocean Research (Ministry of Earth Sciences) for providing funds for purchase and installation of imaging Riometer at Indian Antarctic station, Maitri and all the infrastructural facilities during the Antarctic Expeditions. The authors would also like to acknowledge the CDAWeb for providing ACE satellite data, World Data Center (WDC), Kyoto for geomagnetic indices.

References

1. Abdu, M. A., S. S. Degaonkar, and K. R. Ramanathan, 1967, Attenuation of galactic noise at 25 MHz and 21.3 MHz in the ionosphere over Ahmedabad during 1957–1964, J. Geophys. Res., 72, 1547–1554.
2. Allen, J. H., and H. W. Kroehl, 1975, Spatial and temporal distributions of magnetic effects of auroral electrojets as derived from AE indices, J. Geophys. Res., 80, 3607—end page.
3. Armstrong R.J., Berkey F.T., and Melbye T.,(1977,The day to night ratio in auroral zone Riometer measurements, Planet Space Sci., 25, 1193-1198.

4. Arun, T., A. Dhar, K. Emperumal, and Pathan B. M., 2005, IMF BYdependence of the extent of substorm westward electrojet, J. Earth Syst. Sci, 114, 177-184.
5. Baker D. N., Pulkkinen T.I., Angelopoulos V., Baumjohann W., McPherron R. L., 1996, Neutral Line model of substorms: pas results and present view, J. Geophys. Res., 101,12, 975.
6. Baumjohan W., Kamide Y.,and Nakamura R., 1996, Substorms, Storms, and near-Earth tail, J. Geomagn. Geoelectr., 48, 177-185.
7. Bhonsle R.V. and Ramanathan K.R., 1958, Studies of cosmic radio noise on 25 Mc/s at Ahmedabad, J. Sci. and Ind. Res., 17A, 40-45.
8. Browne S., Hargreaves J. K., and Honary B., 1995,An imaging Riometer for ionospheric studies, Electronics and Communication, 7,209-217.
9. Budden K. G., 1985, The propagation of radio waves, Cambridge University Press, Cambridge.
10. Ellis G. R., 1957, Cosmic radio-noise intensities below 10 Mc/s, J. Geophys. Res., 62, 229-234.
11. Frey, H. U., Mende, S. B., Angelopoulos, V., and Donovan, E. F., 2004, Substorm onset observations by IMAGE-FUV, J. Geophys. Res., 109, A10304
12. Honary F., Marple S.R., Barrath K., Chapman P., Grill M., and Nielsen E., 2011 Digital beam forming imaging Riometer systems, Review of Scientific instruments, 82, 031301(1-13).
13. Hsu, T. –S. and R.L. McPherron, 1998, The main onset of a magnetospheric substorm, Proc. International conference on substorm (ICS-4), edited by S. Kokubun and Y. Kamide, 79-82, Terra Scientific Publishing Company, Tokyo, Lake Hamana, japan,.
14. Jansky, K. G., 1937, Minimum noise levels obtained on short wave radio receiving systems, Proc. IRE, 25, 1517-1530.
15. Kellerman A. C., 2009, On the relationship between auroral absorption, electrojet currents and plasma convection, Ann. Geophys., 27, 473-486.
16. Krishnaswamy S., Detrick D.L. and Rosenberg T., 1985, The inflection point method of determining Riometer quiet day curves, Radio Sci., 20, 123-136.
17. Little C. G., and Leinbach H., 1958, some measurements of high latitude ionospheric absorption using extraterrestrial radio waves, Proc. IRE, 46, 334-348.
18. Little C. G., 1954, High latitude ionospheric observations using extra terrestrial radio waves, Proc. IRE, 42, 1700.

19. Lui A.T.Y., Lopez R.E., Krimigis S.M., McEntire R.W., Zanetii L.J., and Potemra T.A., 1998, A case study of magnetotail current sheet disruption and diversion, Geophysical Research Letters, 15(7), 721-724.

20. Lunetta M. and Abdu M. A., 1971 A Study on the Latitudinal Features of the Ionospheric Absorption Excursion, Revista Brasileira de Física, 1, 369-379.

21. Lusignan, B, 1960, Cosmic noise absorption measurements at Stanford, California, and Pullman, Washington, J. Geophys. Res., 65, 3895-3902.

22. Moro J., 2012, Denardini C.M., Correia E., Abdu M.A., Schuch N.J. and Makita K., A comparision of two different techniques for deriving the quiet day curve from SARINET Riometer data, Ann. Geophys., 30, 1159-1168.

23. Parameswaran K. and Krishnamurthy B. V., 1976, Studies on ionospheric absorption by riometer technique at magnetic equator, Annales de Geophysique,32, 419-427.

24. Rawer K. and Suchy K., 1976, Remarks concerning the dispersion equation of electromagnetic waves in a magnetized cold plasma, J. Atmos. Terr. Phys., 38, 395- 398.

25. Rostoker, G., Geomagnetic indices, 1972, Rev. Geophys. Space Phys., 4, 935-950.

26. Singh, A. K., Sinha, A. K., Rawat, R. Jayashree, B., Pathan, B. M., and Dhar, A., (2012) A broad climatology of very high latitude substorms, Adv. Space Res., 50, 1512-1523.

27. Stauning P., 1984, Absorption of cosmic noise in the E-region during electron heating events. A new class of Riometer absorption events, 46, 395-398.

28. Steiger W.R. and Warmick J.W., 1961, Observations of cosmic radio noise at 18 Mc/s in Hawaii, J. Geophys. Res., 66, 57-66,.

29. Tanaka Y., Makita K., Nishino M., and Ookawa T., 2007, Development of data analysis program for imaging Riometerby using MATLAB, Bulletin of science and engineering, Takushoku University, 10, 61-66.

30. Vichare G., Rawat R., Hinchanal A., Sinha A.K., Dhar A., and Pathan B.M., 2012, Seasonal evolution of S_q current system at sub-auroral latitude, Earth Planets Space, 64, 1023-1031.

31. Wrenn G. L., Rodger A.S. and Rishbeth H., 1987, Geomagnetic storms in the Antarctica F-region. I. Diurnal and seasonal patterns for main phase effects., J. Atmos. Terr. Phys., 49, 901-913.

Case Studies on Cosmic Noise Absorption At Maitri During Thirtieth Indian Scientific Expedition To Antarctica

Jayanta K. Behera [1*], Ashwini K. Sinha [1], Ajay Dhar [1], Sachin Labde [1] and K. Jeeva [3]

[1] Indian Institute of Geomagnetism, New Panvel (W), Navi Mumbai 410 218, India.

[2] National Centre for Antarctica and Ocean Research, Headland Sada, Vasco-da-Gama, Goa 403 804, India.

[3] Equatorial Geophyscal Research Laboratory, VittalapuramVilakku, Krishnapuram, Maharajanagar, Tirunelveli 627 011, India.

Abstract

Cosmic noise absorption ((CAN) at high latitudes is a typical manifestation of enhanced precipitation of energetic charged particles during the course of a magnetospheric substorm. Present analysis demonstrates the energetic particles precipitate to the high latitude ionosphere during subtorms, affecting upper and lower regions of the ionosphere simultaneously. Previous studies have reported that intense and short-lived CNA events associated with substorms are mostly observed in the midnight sector of the auroral oval. In the current study, we have examined such type of CNA events predominantly occurring during 0000-0600 UT (2300-0500 MLT) at an Indian Antarctic station Maitri (corrected geomagnetic (CGM) coordinates 62.59^0 S, 53.59^0 E), which is located at the equatorward edge of the auroral oval. Absorption events related to isolated substorm and storm-time substorms exhibit distinct features in terms of their intensity and extent in latitude and longitude. Our study suggests that the maximum intensity of CNAs depends on the interplanetary conditions, such as, the solar wind speed, southward component of IMF *Bz*, and duskward component of IEF *Ey*. Moreover, the role of duskward component of IEF E*y* is more noteworthy than other interplanetary parameters.

Keywords: *Cosmic noise absorption, Imaging Riometer, Substorm, Geomangetic storm*

1. Introduction

The disturbance created in the auroral ionosphere by precipitation of energetic particles during different processes has been of immense interest for the polar researchers (e.g., Newell and Meng, 1992; Burns et al. 1990; Meredith et al., 2011; Wing et al., 2013, etc.]. Magnetospheric substorms are known to populate nightside

inner magnetosphere and auroral ionosphere with electrons and ions of wide energy ranges [Birn et al, 1997; Wing et al., 2013]. Effects of enhanced population of energetic particles have been extensively studied using ground and satellite based observations [e.g., Arnoldy, 1974; Sotirelis et al., 2013 and references therein].

The energies of softer electrons (energy < 10 keV) precipitating to the auroral ionosphere are absorbed in the E and F regions of the ionosphere and create magnificent optical auroral emissions. Additionally, low energy electrons enhance the auroral currents (electrojets) that can be easily monitored through magnetometers. Electrons of harder energies (> 20 keV) reach to the D region of the auroral ionosphere [Wilson and Stoker, 2002; Baker et al., 1982; Meredith et al., 2011]. Transient changes of harder electron densities in the lower ionosphere could additionally be monitored by Riometer (***R***elative ***I***onospheric ***O***pacity ***meter***). Incoming intergalactic cosmic radio waves to the Earth are absorbed to different degrees while passing through the ionosphere depending upon electron densities [Hargreaves, 1969]. Thus, cosmic noise absorption (CNA) provides an indirect method for diagnostics of the state of the ionosphere. Moreover, the total energy budget entered into the magnetosphere can be simultaneously monitored by PC-index and CNA, as it has been observed that CNA is unanimously dependent upon the geomagnetic activity level, which is characterized by PC-index [Alexander Frank-Kamenetesky and Oleg Troshichev, 2011].Various types of CNAs are commonly observed, e.g., F-region absorption, sudden cosmic noise absorption (SCNA), polar cap absorption (PCA), Auroral Substorm Absorption (ASA), dayside absorption spike events, poleward progressing absorption (PPA), etc., it is often possible to distinguish different types of absorption events on the basis of their appearances in the recordings of absorption intensities combined with knowledge of latitude, local time and season during the observations [Stauning, 1996].

Magnetospheric substorms initiate near midnight [Akasofu, 1968; Singh et al., 2012], as a result of which associated CNA events are often observed in the midnight sector of the auroral region during different phases of auroral substorms [Hargreaves, 1974; Jussila et al., 2004]. Generally, night-time CNA events are produced due to the precipitation of energetic electrons along the field lines from the injection region. However occasionally substorm associated CNA events are observed towards morning or even noon sectors due to eastward drift of electrons [Kavanagh et al., 2002; Birch et al., 2013].

Numerous studies on the substorm-associated CNAs have been carried out in the past using wide as well as narrow beam riometers [Ranta et al., 1981; Nielsen, 1980; Kikuchi et al., 1990]. With further advancement in instrumentation, multi-narrow-beam imaging riometers [Detrick and Rosenberg, 1990; Browne et al., 1995] were utilized to study the dynamics of substorms and CNA signatures on a relatively smaller spatial scale [Kavanagh, 2002; Kellerman and Makarevich, 2011; Hargreaves et al., 1997].

It has been reported that CNAs exhibit distinct features during different phases of a substorm, e.g., reduction in CNA during the growth phase due to the stretching of field lines and enhancement preceding substorm onset by a few minutes due to the dipolarization [Kellerman and Makarevich, 2011]. Dispersionless plasma injections into the inner magnetosphere are typical feature of a substorm onset [e.g., Birn et al, 1997]. CNA observed by a suitably located riometer has been demonstrated to be an effective tool for ground-based identification of dispersionless electron injections [Spanswick et al., 2007].

Electromagnetic and plasma properties in the near-Earth environment are closely related to changes in the solar wind parameters, e.g., southward orientation of the interplanetary magnetic field (IMF *Bz*) drive storms and substorms [Kullen and Karlsson, 2004; Gonzalez and Tsurutani, 1987], high speed solar wind streams generate HILDCAA events [Tsurutani and Gonzalez, 1987], pressure pulse compresses the magnetosphere and induce auroras [Liou et al., 2007], etc. CNA variations in response to the changes in the interplanetary conditions have been extensively examined [Meredith, et al., 2011; Korotova et al., 1997; Behera et al., 2014].

In this study, we have examined substorm-associated CNA absorptions observed at an Indian Antarctic station – Maitri (MLAT ~ 62^{o} S) in relation to the interplanetary conditions. Our station being located towards the equatorward boundary of the auroral oval [Hanchinal et al, 1996], occurrences of substorm associated typical signatures of magnetic variations and CNAs are relatively less frequent in comparison to those identified by AL negative bays.

2. Data set and event selection

A 38.2 MHz (4 x 4 system) was installed at Indian Antarctic station, Maitri (Geographic coordinates: 70.75°S, 11.73°E; CGM coordinates: 62.59°S, 53.59°E; L=5; MLT ≈ UT – 1) during the austral summer 2009-2010. Further details on the riometer system can be found in Behera et al. [2014]. In the present study, riometer and digital fluxgate magnetometer (DFM) data from Maitri have been used for the period November 2010 to October 2011 when both instruments were simultaneously operational. Location of Maitri is such that it comes under the influence of Sq currents during geomagnetic quiet conditions [Vichare et al., 2012] whereas during disturbed conditions auroral electrojets determine geomagnetic field variations at Maitri [Arun et al., 2005].

For identification of substorm events, we used the conventional AL index available from the webpage of WDC, Kyoto (http://wdc.kugi.kyoto-u.ac.jp/aeasy/index.html). During the local night time at Maitri (2300-0500 MLT), AL, H-component variations at Maitri (MAI-H) and absorption data were visually scanned over the selected interval for selection of events. Maitri being in the southern hemisphere (in opposite hemisphere of AL stations) and near equatorward boundary of the auroral oval, AL

negative bays are not always evident or comparable with MAI-H. Only those events were considered as substorm absorptions events for which sharp AL negative bay attained values < -150 nT followed by concurrent westward electrojet signature (MAI-H < - 70 nT) over Maitri and CNA > 0.2 dB. We ignored cases when there were significant (more than 15 minutes) delays between the onsets of MAI-H depression and CNA absorption.

We identified 31 clear substorm absorption events at Maitri over the selected one year duration. Fig. 1 shows distribution of events during magnetic local night hours. Events are mostly confined to pre-midnight and early dawn hours and this may be attributed to substorms primarily occurring around magnetic mid-night hours and the location of Maitri. We additionally examined SYM-H index during the selected events. It was observed that 26 absorption events occurred during moderate to weak storms (SYM-H < -30 nT), whereas only 5 events were not related to storm (SYM-H > -30 nT).

In order to examine the selected events in relation to interplanetary conditions, we used IMF and solar wind data obtained from OMNIWeb (http://omniweb.gsfc.nasa.gov/form/omni_min.html),. OMNIWeb data are time shifted to the bowshock nose considering the travel time of solar wind from the location of observation [e.g., Weimer and King, 2008].

For the selected events, correlations among the intensities of the global AL index, MAI-H and CNA over Maitri have been shown in Fig. 2. Magnitudes of maximum depressions in the AL index (Max |AL|) and MAI-H (Max |H|), and corresponding maximum enhancement in CNA (Max (CNA)) were estimated for each event. The scatter plots for Max |AL| vs Max |H| (correlation coefficient, r = 0.86), Max |H| vs Max (CNA) (r = 0.79) and Max |AL| vs Max (CNA) (r = 0.67) have been shown in Fig. 2. This ensures that the selected absorption events are associated with substorms.

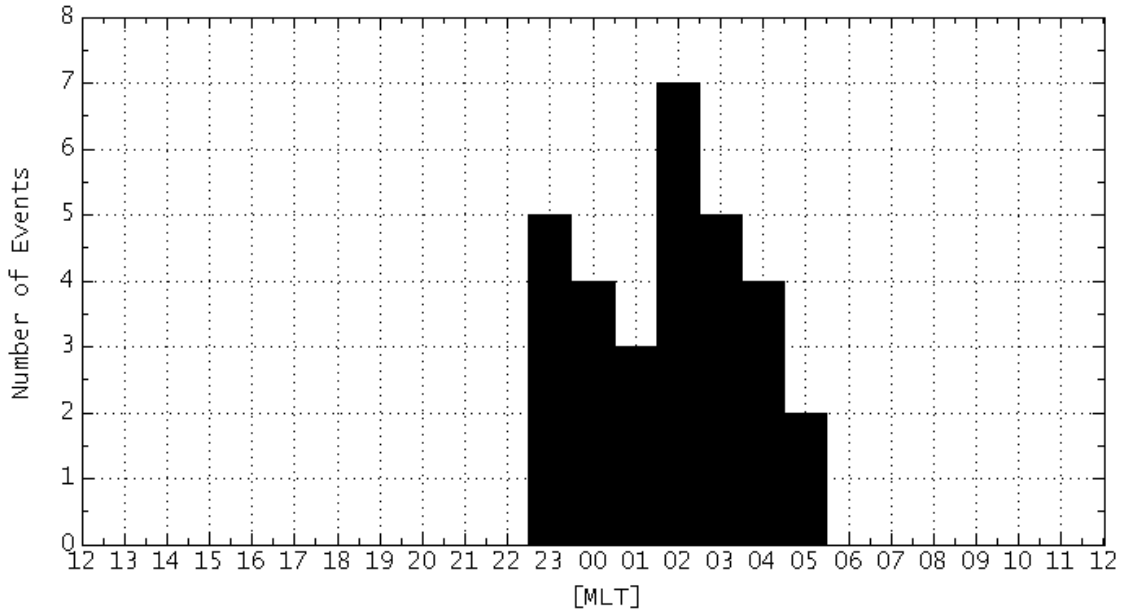

Figure 1*: MLT distribution of onset of westward electrojet and CNA events for selected events at Maitri, Antarctica. Occurrence peaks around pre-midnight and early dawn hours.*

Linear relationship between the Max |AL| and Max |H| clearly suggests that during the selected events the maximum intensity of the westward auroral electrojet observed over Maitri during night time varies with substorms intensity observed by the global AL index in the northern hemisphere (Fig. 2a). For the selected events, intensity of CNA at Maitri also changes with varying intensities of the substorms or westward electrojet intensification at Maitri as shown in Figs. 2b and 2c. However, intensity of the absorption is better correlated with MAI-H intensity, which is obvious as both the observations are from the same location. Here, note that we have selected those absorption events which are accompanied by substorms; our figure 2c further demonstrates that being associated with substorms, how CNA varies with AL,

In the following section, we investigate CNA events observed at Maitri in relation to interplanetary conditions.

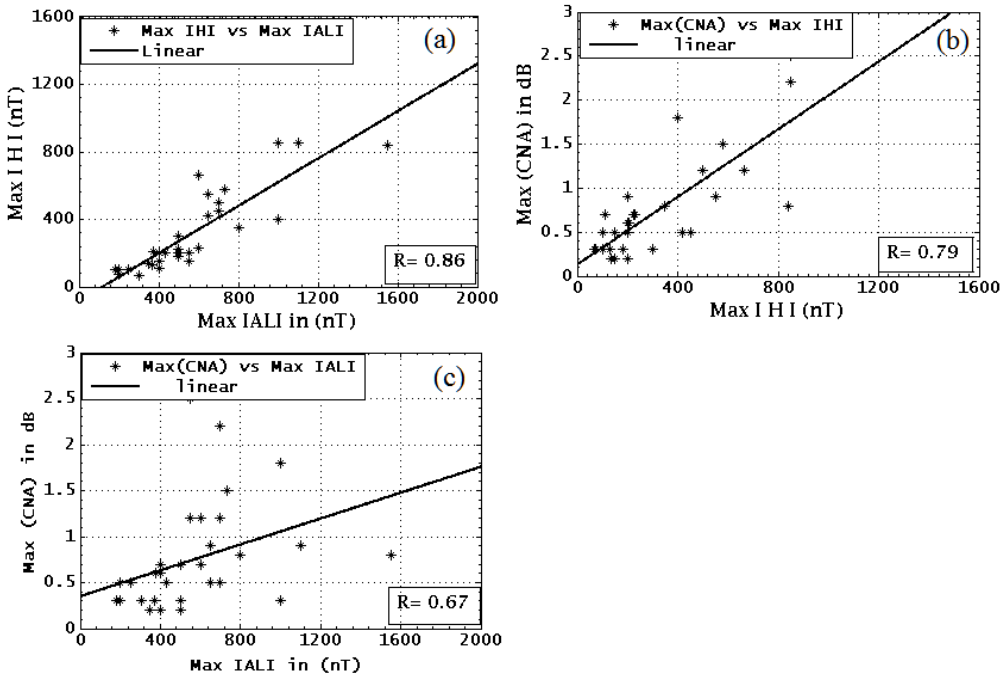

***Figure 2**: Scatter plot of the maximum intensities of (a) AL index vs MAI-H (correlation coefficient, r = 0.86), (b) MAI-H vs CNA (r = 0.79) and (c) AL index vs CNA (r = 0.67) for selected events.*

3. Observations

In this section firstly we present two typical CNA events associated with isolated substorms and one typical event associated with storm-time substorm to bring out the characteristic differences beween these two types of CNA events. The description of these events is followed by a subsection dealing with the effect of interplanetary conditions on CNA considering all the 31 events of one year selected as per the criteria mentioned in section 2.

3.1 Case studies

3.1.1 Event of 20 April 2011

A clear absorption event at Maitri was observed in association with an isolated substorm during 0300 – 0600 UT (0200 – 0500 MLT for Maitri). IMF *Bz* and *Vsw* taken from OMNIWeb is shown in the top two panels of Fig. 3. Occurrence of the substorm and its clear signatures in magnetometer and riometer data are evident as shown in the lower panels. Onset of sudden drop in AL leading to a negative bay started around 0410 UT, which appears to coincide with southward turning of IMF *Bz*. *Vsw* was steady (~ 450 km/s) during the event. It may be noted that the AL negative bay lasts longer than the MAI-H depression or CNA enhancement. Moreover, Max |AL| (700 nT) is higher than Max |H| (400 nT) for the event that could either be due to difference in the location of Maitri with respect to substorm onset region or due to the hemispherical asymmetry. Intensity of CNA maximized to about

1.0 dB during the substorm. SYM-H pattern (> -35 nT) suggests that the substorm

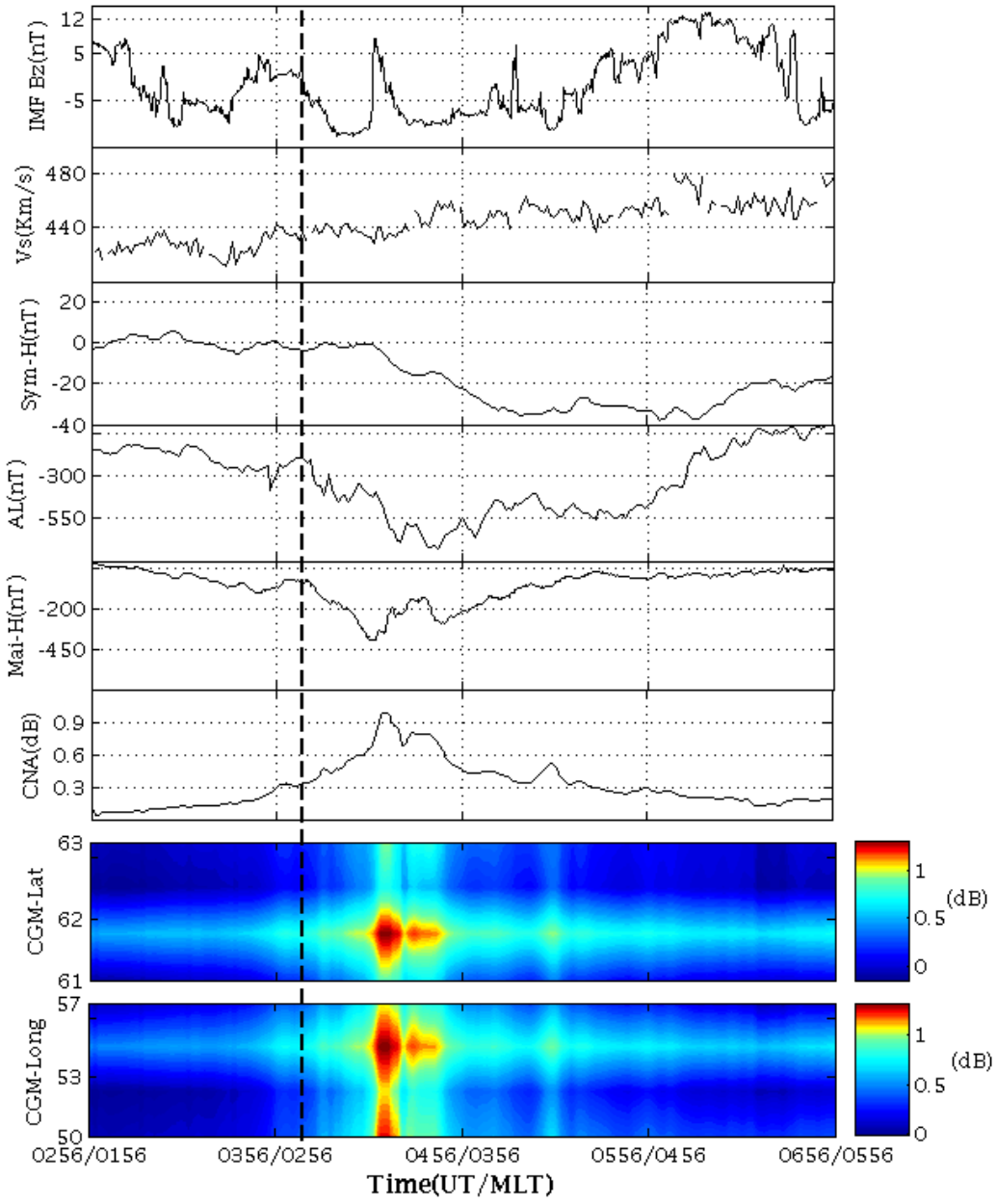

event occurred during a weak storm.

Figure 3*: CNA event at Maitri during an isolated substorm on 20 April 2011. IMF Bz and Vsw are shown in the top two panels. Next, SYM-H is shown (third panel). In response to the AL negative bay (fourth panel), westward electrojet and CNA were clearly observed (fifth and sixth panel). Last two panels show latitude and longitude extent of the absorption.*

The last two panels in Fig. 3 represent latitudinal and longitudinal extent of the absorption for the event of 20 April 2011. Riometer observations show that absorption which in turn indicates particle precipitation maximizes around 62^0 CGM

latitude and the longitudinal extent was over the complete field of view of the Maitri riometer. However the maximum CNA was observed around 55^0 CGM Longitude.

3.1.2 Event of 9 August 2011

A substorm leading to westward electrojet and CNA absorption signatures at Maitri started around 0450 UT. IMF *Bz* and *Vsw* for the event have been shown in the top two panels of Fig. 4. Substorm appears to have initiated with reduction in IMF *Bz*, whereas *Vsw* remained steady. The max |AL| was ~ 600 nT for the event. Maitri was located in dawn hours during the substorm. It can be seen that the westward auroral electrojet extended to Maitri about an hour later from the onset of substorm. Variation in CNA clearly follows MAI-H variation. During the substorm event SYM-H dropped up to -25 nT, thereby suggesting that the event occurred during a very weak storm.

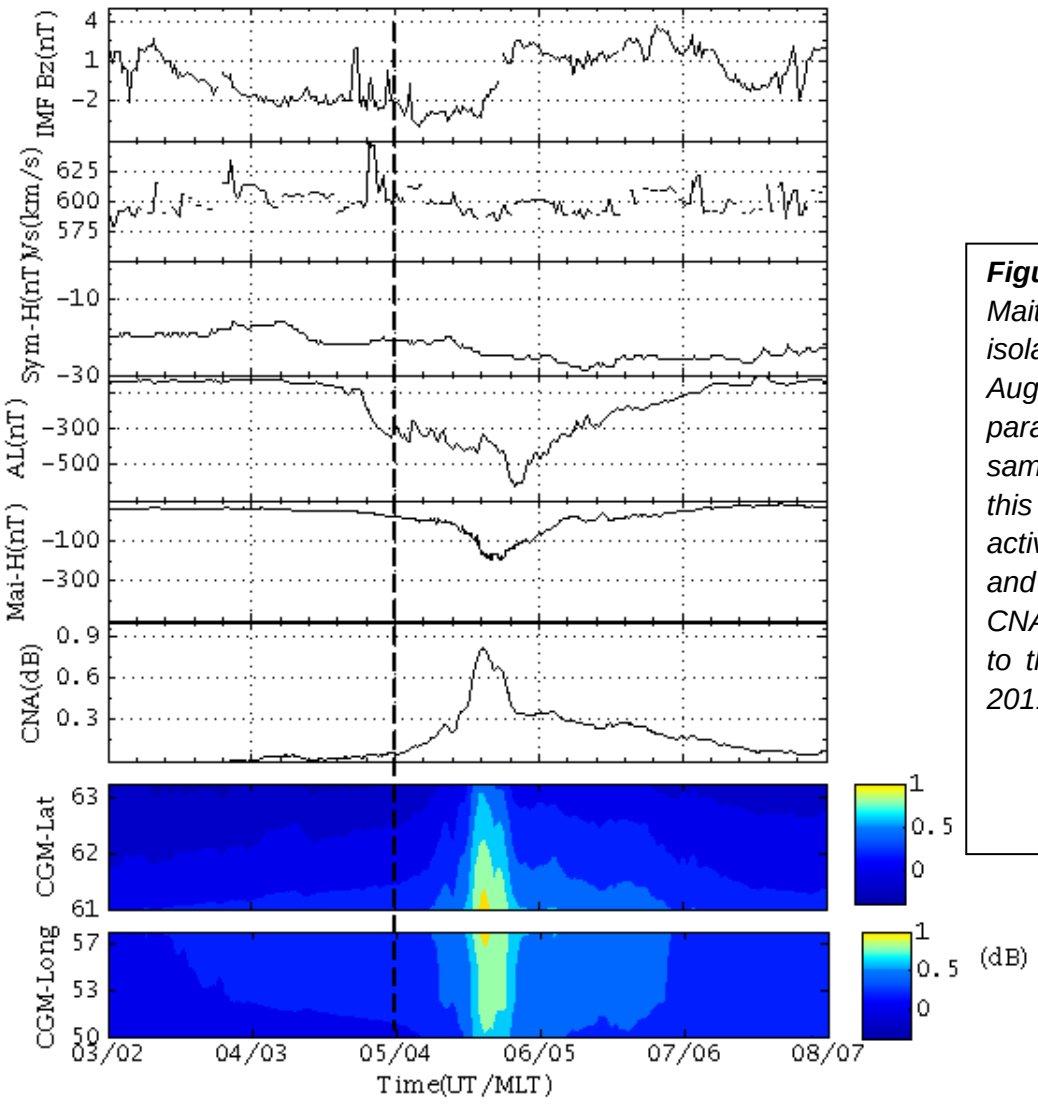

Figure 4*: CNA event at Maitri during another isolated substorm on 9 August 2011. The parameters were plotted same as Fig 3. During this event, the substorm activity was moderate and less production of CNA at Maitri compared to the event on 20 April 2011.*

As shown in the bottom two panels for Fig. 4, precipitation of energetic electrons leading to CNA was mainly localized equatorward of Maitri station. Moreover, CNA was more intense in east longitudes during the event.

3.1.3 Event of 29 May 2011

A very intense storm-time substorm was initiated around 0500 UT, i.e., 0400 MLT for Maitri. The Dst index was ~ -66 nT for the event. AL negative bay started when IMF *Bz* was southward and *Vsw* was quite high (~650 km/s) for the event (Fig. 5). In a way similar to events discussed above, MAI-H or CNA variations lasted for shorter interval in comparison to AL variation. For this intense substorm event (Max |AL| ~ 1000 nT), Max |H| reached to about 800 nT and Max (CNA) exceeded 2 dB at Maitri. Unlike the above two events, SYM-H value relatively reduced more and has gone down to -64 nT during this event.

Several bursts of absorption covering almost the field of view of Maitri imaging riometer system were observed during the substorm as shown in the bottom two panels of Fig. 5.

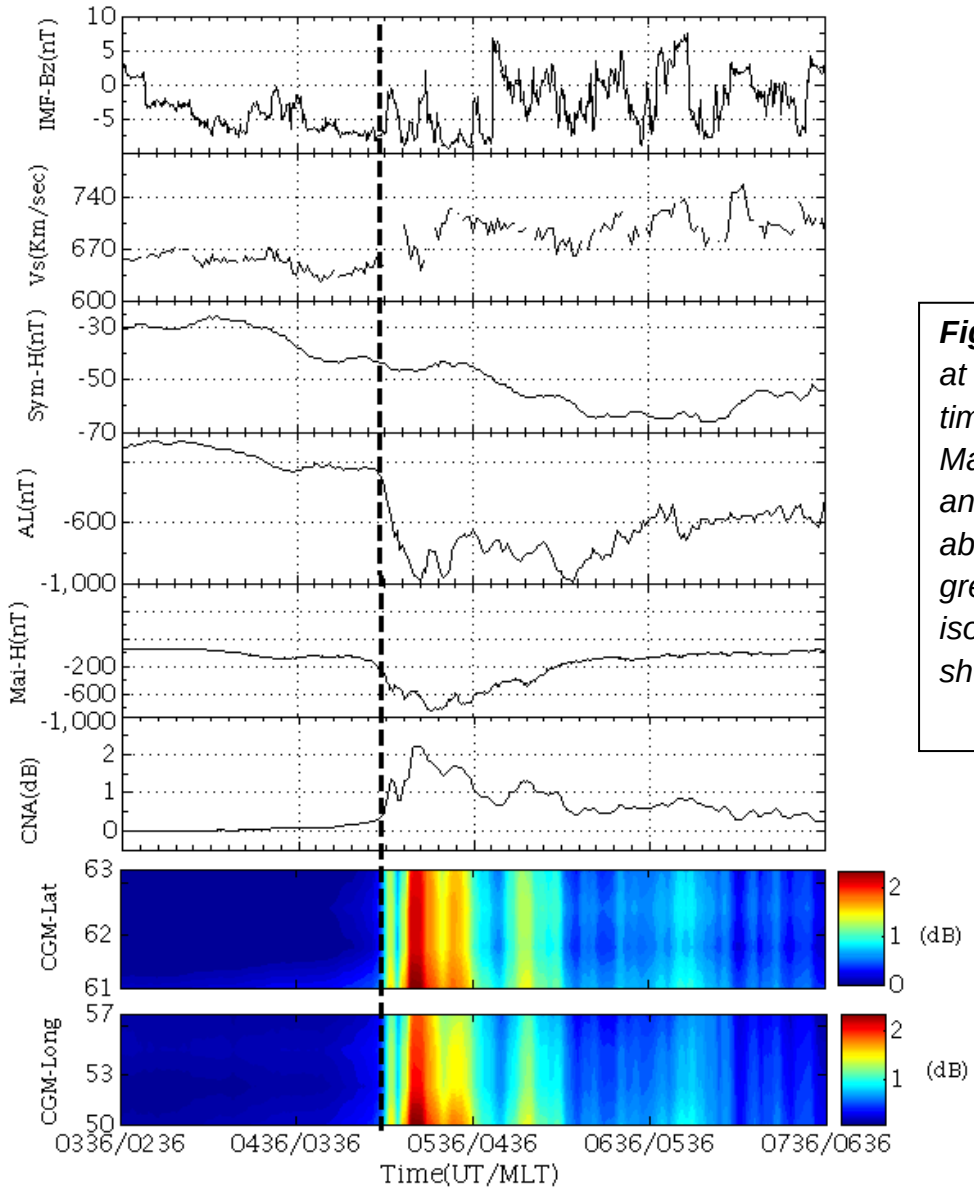

***Figure 5**: CNA event at Maitri for a storm-time substorm on 29 May 2011. Intensity and region of CNA absorption are far greater than those for isolated substorms shown in Figs. 3 and 4*

3.2 Effect of interplanetary conditions on CNAs

Geomagnetic activity is mainly controlled by the southward IMF *Bz*, *Vsw* and dawn-dusk interplanetary electric field, *Ey* (= - *Vsw* x *Bz*). In this section we examine variations of Max |AL|, Max |H| and Max (CNA) for all the selected events in relation to *Bz*, *Vsw* and *Ey*.

In a way similar to the maximum values of |AL|, |MAI-H| and CNA for each event, we calculated the highest magnitudes of southward IMF *Bz* (Max |IMF *Bz*), duskward IMF *Ey* (Max *Ey*) and *Vsw* (Max *Vsw*).

Scatter plots of Max |*Vsw*| vs Max (CNA) (*r* = 0.50), Max |*Bz*| vs Max (CNA) (*r* = 0.75) and Max *Ey* vs Max (CNA) (*r* = 0.85) are shown in Fig. 6. Poor correlation between the maximum *Vsw* and CNA intensity at Maitri suggests that solar wind speed alone does not effectively determine the level of particles precipitation over Maitri (Fig. 6a). However, for higher magnitude of southward IMF Bz during the substorm, precipitation of electrons leading to increased CNA (Fig 6b). Intensity of the absorption is highly correlated with the maximum duskward IMF *Ey* (Fig. 6c). It clearly suggests that the duskward oriented interplanetary electric field was the most important controlling factor for CNAs observed at Maitri.

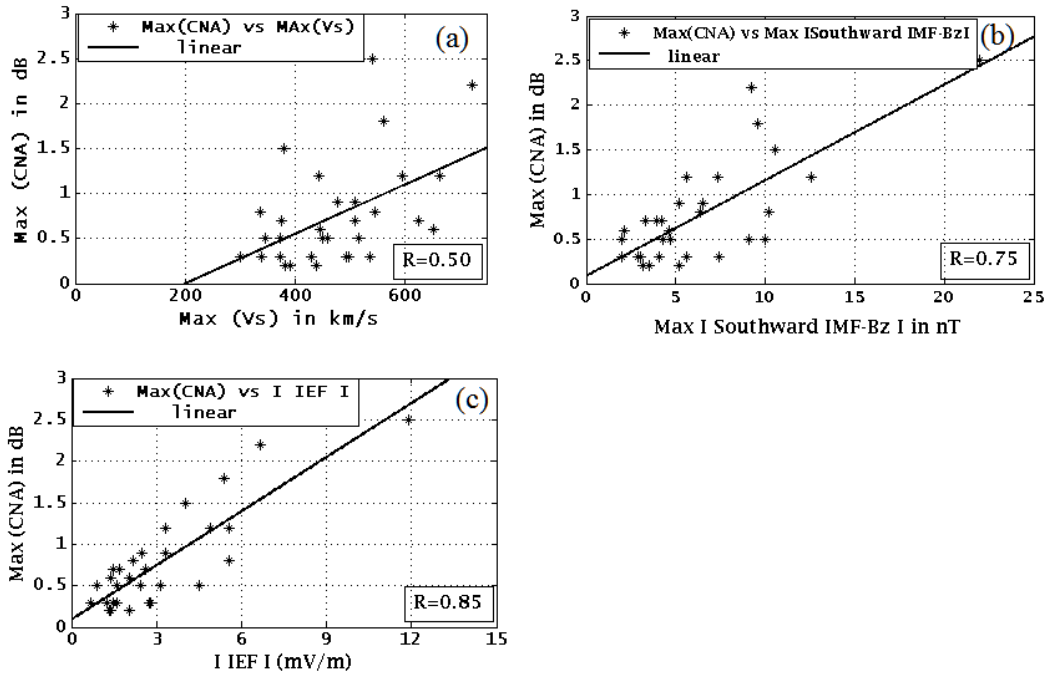

Figure 6*: Scatter plot of the maximum intensities of (a) Vsw vs CNA (correlation coefficient, r = 0.5), (b) southward IMF Bz vs CNA (r = 0.75) and (c) duskward IEF Ey vs CNA (r = 0.85) for selected events. CNA intensity at Maitri has strong dependence on IEF Ey.*

Moreover, for all the selected events IMF *Bz* was southward in the vicinity of onset of AL negative bay. The Max |IMF *Bz*| varied between 2 to 22 nT. Although substorm-associated CNA events occurred during a wide range of southward IMF Bz

conditions, figure (6b) clearly shows most of the events were observed when IMF Bz was weakly southward. For the selected events, the Max |*Vsw*| varied from about 300 to 725 km/s (Fig. 6a). It is observed that the occurrence of absorption events at Maitri, however, do not have strong dependence on the solar wind speed.

4. Results and discussion

Precipitation of energetic electrons into the auroral ionosphere usually affect different regions depending upon their energies, e.g., westward auroral electrojet is driven by low energy electrons precipitated in the E-region, whereas higher energy electrons lead to cosmic radio noise absorption in the D-region [Wilson and Stoker, 2002; Baker et al., 1982]. During magnetospheric substorms (as identified by the AL index), we selected 31 associated events at Maitri based on concurrent response in the magnetometer and riometer data. Substorm-associated CNA events were mainly localized near local midnight, which is consistent with earlier observations [e.g., Kellerman and Makarevich, 2011].

The maximum intensities of MAI-H and CNA at Maitri were well correlated with the intensity of AL index (Fig. 2). However, we observed that the MAI-H negative bays were short-lived and corresponding maximum intensities (max |H|) were consistently lower than those for AL negative bays as shown in Figs. 3-5. AL index being the lower envelop of H component disturbance from about 10-12 stations [Davis and Sugiura, 1966], negative bay could last longer due to contributions from other stations where westward electrojet maximizes. Moreover, hemispherical asymmetry in the substorm signatures [Weygand and Zesta, 2008; Singh et al., 2012] and the location of Maitri station (equatorward of auroral oval in the southern hemisphere) could be other reasons for the difference between AL and MAI-H signatures.

High correlations of Max |H| vs Max (CNA) (Fig. 2b), and MAI-H vs CNA for individual substorm events (see Figs. 3-5) clearly suggest that softer and harder energy electrons, respectively affecting upper and lower regions of the ionosphere, simultaneously precipitate to the auroral ionosphere during sustorms.

Isolated and storm-time substorms mainly differ by the magnitude and extent [Feldstein et al., 2006; Partamies et al., 2013]. It is evident from Figs. 3 and 4 that for isolated substorm events, absorptions over Maitri were quite localized in latitude (< 2 degrees), but fairly wide in longitude (about 5 degrees). For storm-time substorm absorption was much intense and covers the entire field of view of the riometer (Fig. 5).

At Maitri station, most of the substorm-associated CNA events (26 out of 31) were observed during moderate to weak magnetic storms and predominantly under southward IMF *Bz* conditions . Studies based on the simultaneous particle flux data from NOAA POES satellite and Imaging riometer data from Kilpisjarvi (69.05^0 N, 20.79^0 E, geographic coordinates) suggest that the intensity and local time of the particle precipitation and CNA change dramatically during high speed streams (HSS)

of the solar wind [Meredith et al., 2011; Kavanagh et al., 2012]. Although our study does not address HSS, we observed that the occurrence frequency of CNA events is independent of the speed of solar wind (Fig. 6a). Nevertheless, there is an indication of increased CNA intensity with increasing solar wind speed. Intensity of southward IMF *Bz* during the substorms clearly increased the level of absorption at Maitri (Fig 6b). It is consistent with the finding of Kavanagh et al. [2004; 2012] that negative IMF *Bz* produces higher CNA across all L-shells and MLT.

The dawn-dusk component of the interplanetary electric field (*Ey*), which depends on solar wind speed and IMF *Bz*, is known to be extremely important for driving geomagnetic activity [e.g., Huang et al., 2005; Chakrabarty et al., 2008]. Maximum intensity of absorption at Maitri (Max (CNA)) almost linearly increased with increasing duskward IEF *Ey* intensity as shown in Fig. 6c.

5. Summary and conclusions

Our analysis of about 1 year magnetometer and riometer data of Maitri station, Antarctica in relation to magnetic substorms and interplanetary conditions suggests that:

1. Onsets of the westward electrojet and cosmic noise absorption at the station were centered around local midnight. Intensity of the electrojet and CNA over Maitri were almost linearly related to the intensity of (northern hemispheric) AL index.
2. At Maitri, westward electrojet and cosmic noise absorption were mainly observed during storm-time substorms possibly due to the location of the station near equatorward boundary of the auroral oval.
3. A clear distinction in the intensity and extent of the absorption region was observed for isolated substorm and storm-time substorm cases. Usually storm-time substorm absorption events were far more intense and covered wide latitude and longitude regions.
4. Magnitudes of the southward IMF *Bz* or duskward IEF *Ey* were linearly related to intensity of CNA at Maitri. Moreover, increasing solar wind speed and IMF *Bz* appear to cause enhancement in the precipitation of harder electrons leading to enhanced CNA.

Acknowledgment:

Authors would like to extend their sincere thanks to the National Centre for Antarctica and Ocean Research (Ministry of Earth Sciences) for providing the necessary infrastructure during the XXXIII Indian Scientific Expedition to Antarctica, 2011. Authors also acknowledge the OMNIWeb (http://omniweb.gsfc.nasa.gov/form/omni_min.html) for time-shifted interplanetary

observations and World Data Centre (WDC), Kyoto (http://wdc.kugi.kyoto-u.ac.jp/aeasy/index.html) for geomagnetic indices.

References

1. Akasofu, S.-I. Polar and magnetospheric substorms, D. Reidel, Dordrecht, Holland, 1968.
2. Arnoldy, R. L. Auroral particle precipitation and Birkeland Currents. Rev. Geophys. 12(2), 217–231, doi:10.1029/RG012i002p00217, 1974.
3. Alexander Frank-Kamentsky and O. Troshichev, A relationship between the auroral absorption and the magnetic activity in the polar cap. Journal of Atmospheric and Solar-Terrestrial Physics, 77, 40-45, 2011.
4. Arun T., Dhar, A., Emperumal, K., Pathan, B. M. IMF BY dependence of the extent of substorm westward electrojet. J. Earth Syst. Sci. 114, 177–184, 2005.
5. Baker, D. N., Hones, E. W., Belian, R. D., Higbie, P. R., Lepping, R. P., Stauning, P. Multiple-spacecraft and correlated riometer study of magnetospheric substorm phenomena. J. Geophys. Res. 87, 6121-6136, doi:10.1029/JA087iA08p06121, 1982.
6. Behera, J. K., Sinha, A. K., Singh, A. K., Rawat, R., Vichare, G., Dhar, A., Pathan, B. M., Nair, K. U., Selvaraj, C., Elango, P. First results from imaging riometer installed at Indian Antarctic station Maitri. J. Earth Syst. Sci. 123(3), 593-602, 2014.
7. Birch, M. J., Hargreaves, J. K., Bromage, B. J. I. Properties of auroral radio absorption patches observed in the noon sector using imaging riometer and incoherent-scatter radar. J. Atmos. Sol. Terr. Phys. 105-106, 262–272, 2013.
8. Birn, J., Thomsen, M. F., Borovsky, J. E. Reeves, G. D., McComas, D. J., Belian, R. D. Characteristic plasma properties during dispersionless substorm injections at geosynchronous orbit. J. Geophys. Res., 102(A2), 2309–2324, doi:10.1029/96JA02870, 1997.
9. Browne, S., Hargreaves, J. K., and Honary, B.: An imaging riometer for ionospheric studies, Electronics and Communication, 7, 209-217, 1995.
10. Burns, C. J., Howarth, W. G., Hargreaves, J. K. High-resolution incoherent scatter radar measurements during electron precipitation events. J. Atoms. Terres. Phys. 52 (3), 205-218. 1990.
11. Chakrabarty, D., Sekar, R., Sastri, J. H., Ravindran, S. Distinctive effects of interplanetary electric field and substorm on nighttime equatorial F layer: A case study. Geophys. Res. Lett. 35, L19108, doi:10.1029/2008GL035415, 2008.

12. Davis, T., Sugiura, M. Auroral electrojet activity index ae and its universal time variations. J. Geophys. Res. 71, 785–801, 1966.

13. Detrick, D. L., Rosenburg, T. J. A Phased-Array Radio wave Imager for Studies of Cosmic Noise Absorption. Radio Sci. 25, 325–338, 1990.

14. Feldstein, Y. I., Popov, V. A., Cumnock, J. A., Prigancova, A., Blomberg, L.G., Kozyra, J. U., Tsurutani, B. T., Gromova, L. I., Levitin, A. E. Auroral electrojets and boundaries of plasma domains in the magnetosphere during magnetically disturbed intervals. Ann. Geophys. 24, 2243-2276, 2006.

15. Gonzalez, W. D., Tsurutani, B. T. Criteria of interplanetary parameters causing intense magnetic storms (Dst < -100 nT). Planet. Space Sci. 35, 1101–1109, 1987.

16. Hargreaves, J. K. Auroral Absorption of HF Radio Waves in the Ionosphere: A Review of Results from the First Decade of Riometry. Proceedings of the IEEE, 57, 1348–1373, 1969.

17. Hargreaves, J. K. Dynamics of auroral absorption in the midnight sector - The movement of absorption peaks in relation to the substorm onset. Planet. Space Sci. 22, 1427–1441, 1974.

18. Hargreaves, J. K., Browne, S., Ranta, H., Ranta, A., Rosenberg, T. J., Detrick, D. L. A study of substorm-associated nightside spike events in auroral absorption using imaging riometers at South Pole and Kilpisjärvi. J. Atmos. Sol. Terr. Phys., 59 (8), 853–872, 1997.

19. Hanchinal, A.H, Jeeva, K., Ajay Dhar and Girija Rajaram. Response of Geomagnetic Field at Indian Antarctic Station Maitri, to increasing Electromagnetic disturbance in Geospace. Technical Publication (Twelfth Indian Expedition to Antarctica), 10, 47-57,1996.

20. Huang, C.-S., Foster, J. C., Kelley, M. C. Long-duration penetration of the interplanetary electric field to the low-latitude ionosphere during the main phase of magnetic storms. J. Geophys. Res. 110, A11309, doi:10.1029/2005JA011202, 2005.

21. Jussila, J. R. T., Aikio, A. T., Shalimov, S., Marple, S. R. Cosmic radio noise absorption events associated with equatorward drifting arcs during a substorm growth phase. Ann. Geophys. 22, 1675–1686, 2004.

22. Kavanagh, A. J. Energy deposition in the lower auroral ionosphere through energetic particle precipitation. Ph. D. Thesis, Univ. of Lancaster, Lancaster, U. K, 2002(a).

23. Kavanagh, A. J., Honary, F., McCrea, I. W., Donovan, E., Woodfield, E. E., Manninen, J., Anderson, P. C. Substorm related changes in precipitation in the dayside auroral zone – a multi instrument case study, Ann. Geophys. 20, 1321–1334, 2002(b).

24. Kavanagh, A. J., Kosch, M. J., Honary, F., Senior, A., Marple, S. R., Woodfield, E. E., McCrea, I. W., The statistical dependence of auroral absorption on geomagnetic and solar wind parameters. Ann. Geophys. 22, 877-887, 2004.

25. Kavanagh, A. J., Honary, F., Donovan, E. F., Ulich, T., Denton, M. H. Key features of >30 keV electron precipitation during high speed solar wind streams: A superposed epoch analysis. J. Geophys. Res. 117, A00L09, doi:10.1029/2011JA017320, 2012.

26. Kellerman, A. C., Makarevich, R. A. The response of auroral absorption to substorm onset: Superposed epoch and propagation analyses. J. Geophys. Res. 116, A05312, doi:10.1029/2010JA015972, 2011.

27. Kikuchi, T., Yamagishi, H., Lester, M. Drift of auroral absorption due to the magnetospheric convection observed with the scanning narrow beam riometer during SUNDIAL. Ann. Geophys. 8, 431-440, 1990.

28. Korotova, G. I., Sibeck, D. G., Rosenberg, T. J., Russell, C. T., Friis-Christensen, E. High-latitude ionospheric transient events in a global context. J. Geophys. Res. 102(A8), 17499–17508, doi:10.1029/97JA00939, 1997.

29. Kullen, A., Karlsson, T. On the relation between solar wind, pseudobreakups, and substorms. J. Geophys. Res. 109, A12218, doi:10.1029/2004JA010488, 2004.

30. Liou, K., Newell, P. T., Shue, J.-H., Meng, C.-I., Miyashita, Y., Kojima, H., Matsumoto, H. “Compression aurora”: Particle precipitation driven by long-duration high solar wind ram pressure. J. Geophys. Res. 112, A11216, doi:10.1029/2007JA012443, 2007.

31. Meredith, N. P., Horne, R. B., Lam, M. M., Denton, M. H., Borovsky, J. E., Green, J. C.. Energetic electron precipitation during high-speed solar wind stream driven storms. J. Geophys. Res. 116, A05223, doi:10.1029/2010JA016293, 2011.

32. Newell, P. T., Meng, C.-I. Mapping the dayside ionosphere to the magnetosphere according to particle precipitation characteristics. Geophys. Res. Lett. 19 (6), 609-612, 1992.

33. Nielsen, E. Dynamics and spatial scale of auroral absorption spikes associated with the substorm expansion phase. J. Geophys. Res. 85, 2092–2098, 1980.

34. Partamies, N., Juusola, L., Tanskanen, E., and Kauristie, K. Statistical properties of substorms during different storm and solar cycle phases. Ann. Geophys. 31, 349-358, doi:10.5194/angeo-31-349-2013, 2013.

35. Ranta, H., Ranta, A., Collis, P. N., Hargreaves, J. K. Development of the auroral absorption substorm: Studies of pre-onset phase and sharp onset using an extensive riometer network. Planet. Space Sci. 29, 1287-1313, 1981.

36. Singh, A. K., Sinha, A. K., Rawat, R., Jayashree, B., Pathan, B. M., Dhar, A. A broad climatology of very high latitude substorms. Adv. Space Res. 50, 1512-1523, doi:10.1016/j.asr.2012.07.034, 2012.

37. Sotirelis, T., Korth, H. Hsieh, S.-Y., Zhang, Y., Morrison, D., Paxton, L. Empirical relationship between electron precipitation and far-ultraviolet auroral emissions from DMSP observations. J. Geophys. Res. Space Physics. 118, 1203–1209, doi:10.1002/jgra.50157, 2013.

38. Spanswick, E., Donovan, E., Friedel, R., Korth, A. Ground based identification of dispersionless electron injections. Geophys. Res. Lett. 34, L03101, doi:10.1029/2006GL028329, 2007.

39. Stauning, P. Investigations of ionospheric radio wave absorption processes using imaging riometer techniques. J. Atmosp. Terr. Phys. 58 (6), 753-764, 1996.

40. Tsurutani, B. T., Gonzalez, W. D. The cause of high-intensity long-duration continuous AE activity (HILDCAAs): Interplanetary Alfvén wave trains. Planetary Space Sci. 35, 405-412, 1987.

41. Vichare, G., Rawat, R., Hinchanal, A., Sinha, A. K., Dhar, A., Pathan, B. M. Seasonal evolution of Sq current system at sub-auroral latitude. Earth Planets Space. 64, 1023-1031, 2012.

42. Weygand, J. M., Zesta, E. Comparison of auroral electrojet indices in the Northern and Southern Hemispheres. J. Geophys. Res. 113, A08202, doi:10.1029/2008JA013055, 2008.

43. Weimer, D. R., King, J. H. Improved calculations of interplanetary magnetic field phase front angles and propagation time delays. J. Geophys. Res. 113, A01105, doi:10.1029/2007JA012452, 2008.

44. Wilson, A., Stoker, P. H. Imaging riometer observations on energetic electron precipitation at SANAE IV, Antarctica. J. Geophys. Res. 107 (A10), 1268, doi:10.1029/2000JA000463, 2002.

45. Wing, S., Gkioulidou, M., Johnson, J. R., Newell, P. T., Wang, C.-P., Auroral particle precipitation characterized by the substorm cycle. J. Geophys. Res. 118, 1022–1039, doi:10.1002/jgra.50160, 2013.

J Opt
https://doi.org/10.1007/s12596-022-01005-9

RESEARCH ARTICLE

Optical studies of low-birefringence liquid crystal solutions using a multi-wavelength hollow prism refractometer

Anita Kanwar[1] · **Vishakha Gajghate**[2]

Received: 9 June 2022 / Accepted: 22 October 2022

Abstract This article presents the study of low-birefringence liquid crystal solution using the multi-wavelength hollow prism refractometer. Phase transition temperatures are measured with Fabry–Perot scattering spectroscopy and an optical polarization microscope. The ordinary and extraordinary refractive indices for two different liquid crystal solutions are measured at three different visible wavelengths and at various temperatures using a hollow prism refractometer. The empirical Cauchy formula is used to investigate the dependence of refractive indices on wavelength. The thermal dependence of the refractive indices is investigated by means of the modified four-parameter model. The values of Cauchy's constants, material constant, thermal variation of birefringence, order parameter, and constants involved in the thermal variation of average refractive index are computed for later application and use. The calculated values for the constants were verified using the experimentally observed values. The anisotropy in the polarizability values of the solution is responsible for the strong temperature dependence of the birefringence, order parameter value, and declining order in the system with the increasing temperature.

Keywords Cauchy model · Birefringence · Order parameter · Polarizability · Vuk's relation and Haller approximation

✉ Anita Kanwar
anita_s_kanwar@yahoo.com

[1] Vivekanand Education Society's College of Arts, Science and Commerce, Sindhi Society, Chembur, Mumbai, Maharashtra 400071, India

[2] Pillai HOC College of Arts, Science and Commerce, Khalapur, HOC Colony Rd, Taluka, Rasayani, Maharashtra 410207, India

Introduction

The liquid crystal state lies between the liquid and crystal state of matter and possesses all the useful properties of liquids and crystals. LCs exhibit anisotropy in their optical, mechanical, thermal, acoustical, electrical, and magnetic properties similar to that of crystals. They also exhibit properties specific to liquids such as fluidity, density, and viscosity. The study of liquid crystals (LCs) is an important subject from the point of research and applications in the display field. The unique optical properties have increased their usage in display. The temperature-dependent refractive index of thermotropic LCs is an optical property, which is of great importance from the application point of view.

Cholesteric liquid crystal (CLC) has a chiral-induced twist in the directors. In the cholesteric phase, the molecules in the different layers are oriented at a slight angle from each other. Each successive molecule is slightly rotated with respect to the previous one. Therefore, instead of the constant director of the nematic, the cholesteric director rotates helically throughout the sample. The CLCs are chosen by many researchers to make temperature-sensitive visible display devices, optical shutters, and photonic bandgap fibres, because of their unique thermal, electrical, and optical properties [1–3]. The cholesteric phase in the liquid crystals is defined in terms of the helical pitch. Helical pitch denotes the distance along the helical axis that corresponds to a 360° rotation in the orientation of rod-type molecules. The periodicity of the cholesteric phase along the helix axis is given by half the pitch. The numerical value of the pitch can vary from a few tens of nanometres to micrometres [4]. Both the numerical value of the pitch and the sign of the twist are influenced by several factors one of which is the type of solvent or dopant. Theoretical explanation and a computational model developed by Kamberaj et al. discuss the same efficiently [5].

Published online: 07 November 2022

Asia-Pacific Financial Markets
https://doi.org/10.1007/s10690-023-09399-7

ORIGINAL RESEARCH

Macroeconomic Response to BRICS Countries Stock Markets Using Panel VAR

Babita Panda[1] · **Ajaya Kumar Panda**[2] · **Pradiptarathi Panda**[3]

Accepted: 18 February 2023

Abstract

This study measures the relationships between macroeconomic variables and stock returns for BRICS countries. The study uses monthly data of select macroeconomic variables collected from February 1997 to December 2019. In addition to the traditional macroeconomic variables, the study used the new age macroeconomic variables like- economic policy uncertainty index, Crude oil volatility index, Global financial stress index, and SENTIX global index. Using Panel VAR and Granger causality, the study finds that market returns positively influence exchange rates. In contrast, the market tends to react negatively to changes in consumer price inflation and foreign portfolio investment. However, the equity market is susceptible to the economic growth (IIP) of BRICS economies. These macroeconomic indicators exhibit significant influence on the stock markets.

Keywords Macroeconomic variables · BRICS stock market · Panel VAR

JEL Classification E60 · G11 · G15

✉ Babita Panda
net2bobby@gmail.com

Ajaya Kumar Panda
akpanda@nitie.ac.in

Pradiptarathi Panda
pradipta.mfc@gmail.com

[1] Pillai HOC College of Arts, Science and Commerce, Rasayani, Raigad, Maharashtra 410222, India

[2] National Institute of Industrial Engineering (NITIE), Powai, Mumbai, Maharashtra 400087, India

[3] National Institute of Securities Markets (NISM), SEBI Road, Patalganga, Rasayani, Raigad, Maharashtra 410222, India

Published online: 09 March 2023

1 Introduction

The process of globalisation has brought the world together. As a result, the response of emerging markets to macroeconomic changes has fascinated global investors. It is because the world has become more integrated than ever. These responses have often created opportunities for portfolio diversification by global investors. Financial openness due to globalisation has opened the financial markets to international investors and increased the risk of contagion. As a result, the world economy has experienced market collapses and economic turmoil due to spillover of financial crises from one market to other. However, spillover of macroeconomic contagion has been observed over a time lag and with varying degrees of intensity.

Nonetheless, globalisation has increased financial integration, resulting in a higher correlation between emerging and global markets (Aloui et al., 2011; Panda et al., 2021). This integration caused diversification of the international portfolio and hedging of potential risk by global investors. Besides, movement in many other macroeconomic variables also impacts the variation in stock prices. Further, economic policy uncertainty index negatively impacts stock markets (Brogaard & Detzel, 2015). Earlier studies find several macroeconomic factors impacting stock market movements. Some indicators are related to real economic activity, such as gross domestic product (GDP) or gross national product (GNP). Since GDP or GNP data are available only quarterly or annually, literature considered the index of industrial production (IIP) as a proxy for GDP or real economic activity in many cases. An expansionary economic activity may be observed with an increase in IIP via increased investment and robust corporate earnings. Higher growth, investment and earnings create positive sentiments leading to an appreciation of stock prices. Studies have reported a positive relationship between IIP and stock price (Chen et al., 1986; Maysami et al., 2004; Rahman et al., 2009; Ratanapakorn & Sharma, 2007). Secondly, an increase in inflationary tendency is a natural phenomenon of a growing economy.

Moreover, inflation is another crucial macroeconomic variable that affects the stock price. Studies find a negative relationship between inflation and stock price (Chen et al., 1986; Fama, 1981; Mukherjee & Naka, 1995; Pal & Mittal, 2011). However, contrary to these studies, Ratanapakorn and Sharma (2007) find a positive relationship between inflation and stock price. Fluctuations in stock prices are considered responses of the markets to external forces. Unexpected events influence individual asset prices, and some affect the stock market more (Chen et al., 1986).

There is a plethora of research on the impact of macroeconomic variables on stock prices. Earlier studies find the existence of positive, negative, and in some cases, no relationship between the traditional macroeconomic variables and stock price. However, studies based on the group of countries are fewer to the best of our knowledge, especially for developing and emerging markets like BRICS countries. Further, studies relating to the impact of new age macro-economic variables on the stock markets are fewer to the best of our knowledge. In this context, the

current study attempts to study the impact of macroeconomic variables and stock prices on BRICS countries. All five economies of BRICS are considered a single unit; hence, the study attempts to analyse a system approach using panel data models. Diversification in these BRICS countries gives economic value (Panda & Thiripalraju, 2020). The external macroeconomic variables spillovers are lower than the internal macroeconomic variables spillovers to the BRICS countries' stock markets (Patra & Panda, 2021). Again, the unconventional monetary policy of the USA and Europe spillovers to the BRICS countries' stock markets (Lubys & Panda, 2021). South Africa is the best country to invest in among the BRICS countries, depending on the risk-reward ratio, followed by Russia, India, Brazil, China, and South Africa. Based on overnight returns, India's risk-reward ratio is higher, followed by Brazil, Russia, and South Africa (Bhuyan et al., 2016). Again, many of the studies have ignored the impact of new-age macroeconomic variables (like the economic policy uncertainty index (EPUI), global economic policy uncertainty index (GEPUI), Crude oil volatility index (CRUDEOIL3M), Global financial stress index (GFSI) and SENTIX global index (SENTIX)) to stock markets. This motivates the present study to consider the new age and traditional macroeconomic indicators to analyse their relative impact on the BRICS stock markets. This study divides macroeconomic variables into two categories (internal and external) to examine their impact on stock markets for BRICS countries.

The study aims to find key systemic indicators that influence the market movements of BRICS using panel data analysis. At the same time, the study also attempts to undertake a series of pre-estimation and post-estimation analyses to ensure robust estimates of the analysis. The BRICS countries are contributing 26% to the world-listed companies, 16% to world market capitalisation, 22% to world GDP, and 42% to the world population. Secondly, these countries are emerging countries attracting foreign investments, and the domestic market capitalisation keeps increasing yearly. This motivates the present research to explore the key systemic indicators influencing its equity market. The present study contributes to the literature in many ways. Unlike previous studies, the present study assumes all five economies of BRICS as one unit (i.e., a single economy unit). It attempts to measure the response of BRICS equity market returns due to macroeconomic shocks specific to BRICS countries and international macroeconomic shocks external to this economy. The study's empirical findings have significant implications for international investors for their portfolio diversification and managing international asset management as well as the policymakers to identify critical systemic factors of the BRIC economy.

Section 2 of this study discusses the literature review; Sect. 3 discusses the nature and sources of data; Sect. 4 highlights methodology, and Sect. 5 presents the study's empirical findings. Lastly, Sect. 6 concludes the study.

2 Literature Review

In this section, the study reviews literature reporting the relationship between macroeconomic variables and stock markets. The existing literature on the impact of macroeconomic variables and stock prices tries to measure the response from real

economic activities, news impact, foreign exchange and interest rate markets, and so on. For instance, news related directly to real activity substantially impacts cyclical stocks more than noncyclical ones. International news impacts more than domestic news on the USA and German stock markets. Considering GDP growth, business confidence measures, and the development of the real sector of the United States and Germany, the study finds news on interest rates, inflation, and the IFO business climate index contribute most to market movements (Funke & Matsuda, 2002). Causality exists between India's stock market and real economic variables (Sahu & Dhiman, 2011). Gold is considered a hedge against stock market volatility. For instance, oil and gold prices negatively impact the stock market, and the money supply positively influences the Indian stock price (Ray, 2012).

Further, UK common stocks offer a hedge against inflation and depend on different inflationary regimes (Narayana & Zheng, 2012). Again, gold and silver can form a reasonably good hedge against stocks (Sireesha, 2013). Sometimes, researchers assess the impact of the foreign exchange market, inflation, and gold on the stock market. For example, inflation and foreign exchange reserves are not impacting the stock price. However, exchange rates and gold prices affect stock prices (Sharma & Mahendru, 2010). During the global financial crisis period, the existence of asymmetric volatility spillovers between stock markets and foreign exchange markets is more (Panda & Deo, 2014a; and 2014b).

The impact of economic forces like the spread between long and short interest rates, expected and unexpected inflation, industrial production, and the spread between high and low-grade bonds are priced in the stock market return of equally weighted as well as value-weighted NYSE index (Chen et al., 1986). Further, the Index of Industrial Production (IIP), net foreign institutional investment (FII), and exchange rate impacted the Indian stock market during the subprime financial crisis. Again, the IIP and exchange rate can predict the stock market better than FII (Mohapatra & Panda, 2012). The long-run relationship exists between the macroeconomic variables and stock markets. For example, IIP, CPI, M1, and Mumbai interbank money market rates have long-run relationships with Indian stock markets.

Further, the IIP impacts positively and inflation negatively on Indian stock markets (Naka et al., 1998). Similarly, studies find that macroeconomic variables help predict the stock markets of several European countries. Further, IIP, inflation, and M1 impact the USA, UK, Germany, Italy, Belgium, France, Netherlands, and Switzerland stock markets (Errunza & Hogan, 1998). Studies find that the short-run and long-run relationship exists between the macroeconomic variables (output, inflation, and interest rates) and stock and bond markets (Dickinson, 2000). Interestingly macroeconomic variables impact the USA stock market positively and negatively in the long run. For example, industrial production, inflation, money supply, short-term interest rate, and exchange rate positively impacts the stock price, and the long-term interest rate is negatively related to the stock price of the USA (Ratanapakorn & Sharma, 2007).

The exchange rate, inflation, money supply, IIP, long-term government bond rate, and call money rate impacts the stock price of Japan in the long run (Mukherjee & Naka, 1995). Further, narrow money supply, broad money supply, and foreign exchange reserves have a long-run relationship with Singapore stock markets, and

the exchange rate does not impact this stock market (Mookerjee & Yu, 1997). Asian countries realise the mixed results on the impact of macroeconomic variables on stock markets. For example, growth in output impacts positively and aggregate price level impacts negatively on the stock markets of the Philippines, Indonesia, Singapore, Malaysia, and Thailand. In addition, a negative relationship exists between stock price and interest rate for the Philippines, Singapore, and Thailand but a positive relationship in the case of Indonesia and Malaysia (Wongbampo & Sharma, 2002). The money supply, GDP, and interest rates explain New Zealand stock markets (Gan et al., 2006). Again, long-run relationships exist between inflation, exchange rate, and the stock markets.

Further interest rates and gross domestic savings do not play a significant role in determining the stock price of India (Pal & Mittal, 2011). Interestingly fiscal deficit and foreign investment are not impacting the Indian stock market. However, interest rate, IIP, money supply, inflation, and exchange rate impact the Indian stock market (Ray & Vani, 2003). The IIP, money supply, and FDI impacts stock prices for India in the long run (Ahmed, 2008). Similarly, a long-run relationship exists between macroeconomic variables and the Indian stock market. Again, a positive relationship exists between money supply and IIP; simultaneously, a negative relationship exists from inflation in the Indian stock market (Naik & Padhi, 2012).

Mixed results on the impact of macroeconomic variables on stock markets realised for Argentina, Brazil, Chile, and Mexico. For example, IIP positively impacts stock markets, and interest rate and exchange rate negatively impact stock markets in Brazil. Further, exchange rate impacts negatively; and IIP, money supply, and interest rates impacts are insignificant. Interest rate and money supply negatively determine Argentina's stock return, and the influence of IIP and exchange rate are insignificant for this market. IIP positively impacts Chile's stock market, and the exchange rate and money supply do not impact these markets (Abugri, 2008).

Similarly, interest rates, foreign exchange reserves, industrial production, money supply and exchange rate negatively impact the Malaysian stock market (Rahman et al., 2009). Further, inflation and stock returns are bidirectionally causing each other (Bhattacharya & Mukherjee, 2006). Again, macroeconomic volatility is not significantly impacting the stock market (Garcia & Liu, 1999). Crude oil and exchange rate for BRIC countries' stock markets are unrelated (Gay, 2008). There is no causality between interest rate and IIP on the stock price. Further, unidirectional causality exists from inflation, FDI, GDP, exchange rate, and fixed capital formation on the stock price. Moreover, bidirectional casualty exists from crude oil price, money supply, foreign exchange reserve, and WPI to stock price exists for India (Ray, 2012).

3 Nature and Data Sources

This study considers monthly internal and external macroeconomic variables and stock indices for each of the BRICS countries. For internal macroeconomic variables, the study considers the IBOVESPA index, the exchange rate (Real), Inflation (CPI), the Index of Industrial Production (IIP), and Net Foreign Portfolio Investment

(FPI) for Brazil. Similarly, for Russia, we have used the MICEX index, the exchange rate (Rubble), Inflation (CPI), the Index of Industrial Production (IIP), and Net FPI. The macroeconomic indicators for India are the NIFTY index, the exchange rate (Rupee), Inflation (CPI), the Index of Industrial Production (IIP), and Net FPI. For China, we have considered the Shanghai Composite Index (SHCOMP), the exchange rate (Yuan), Inflation (CPI), the Index of Industrial Production (IIP), and Net FPI. Finally, for South Africa, we have used JSE all shares index (JALSH), the exchange rate (Rand/ZAR), Inflation (CPI), the Index of Industrial Production (IIP), and Net Portfolio Investment (NPI). Broadly, the country benchmark market index, exchange rate, inflation rate, economic growth proxied as the index of industrial production and net foreign portfolio investments are considered internal country-specific macro indicators. Similarly, as external macroeconomic variables, we have considered the S& P 500 index (SPX), three months crude oil volatility (CO), Global Economic policy uncertainty index (GEPUI), SENTIX Global index (SENTIX), Global Financial Stress Index (GFSI) and Fed Rate (FEDRATE). All data are sourced from Bloomberg, Thomson Reuters, and The Institute of International Finance. The study period is from February 1997 to December 2019, and the frequency of data is monthly. The choice of the study period was based on the maximum availability of the data for each country, and the data period is limited till 2019 as the study does not wish to include the COVID period and the current data period.

4 Methodology

The current study uses dynamic panel data models to measure the dynamic sensitivity of stock market indices of BRICS countries due to internal and external macroeconomic shocks. Since the panel vector autoregression model assumes all the variables should be endogenous to the system of models, the dynamic response of the BRICS stock market indices is estimated through the regression approach of macroeconomic parameters of the whole system. These macroeconomic variables are used as lagged endogenous variables in the system of equations. The estimates of the panel vector auto-regression model (panel VAR) are discussed as follows,

$$\mathrm{SI}_{it} = \sum_{j=1}^{J} \propto_{11j} \mathrm{SI}_{it-j} + \sum_{j=1}^{J} \propto_{12j} \mathrm{EX}_{it-j} + \sum_{j=1}^{J} \propto_{13j} \mathrm{CPI}_{it-j} + \sum_{j=1}^{J} \propto_{14j} \mathrm{IIP}_{it-j} + \sum_{j=1}^{J} \propto_{15j} \mathrm{FPI}_{it-j} + \varepsilon_{1it} \tag{1}$$

$$\mathrm{SI}_{it} = \sum_{j=1}^{J} \propto_{11j} \mathrm{SI}_{it-j} + \sum_{j=1}^{J} \propto_{12j} \mathrm{SPX}_{it-j} + \sum_{j=1}^{J} \propto_{13j} \mathrm{CO}_{it-j} + \sum_{j=1}^{J} \propto_{14j} \mathrm{GEP}_{it-j} + \sum_{j=1}^{J} \propto_{15j} \mathrm{ST}_{it-j} + \sum_{j=1}^{J} \propto_{16j} \mathrm{GF}_{it-j} + \sum_{j=1}^{J} \propto_{17j} \mathrm{FR}_{it-j} + \varepsilon_{1it} \tag{2}$$

where "SI" implies a country-specific stock index, "Ex" represents the exchange rate, "CPI" represents the consumer price index, "IIP" implies the index for industrial production, and "FPI" represents the net foreign portfolio investment for the

respective countries. Similarly, "SPX" implies the S&P 500 index of the USA, "CO" measures three months crude oil volatility index, "GEP" presents the Global Economic policy uncertainty index, "ST" presents the Sentix global index, "GF" represents the Global Financial Stress Index and finally "FR" represents Fed rate. Model 1.1 and 1.2 present reduced form panel VAR model of internal and external macroeconomic variables impacting stock price, respectively. After estimating the reduced form VAR model (i.e., Eqs. 1 and 2), the estimated errors will be modelled in moving average (MA) to capture the impact of endogenous variables. These lagged endogenous variables depend on their estimated lagged residuals of the reduced form VAR model.

As a system of equations, the VAR model estimates equations equal to the number of variables of the model. In the above equation, the subscript *J* implies the optimum lag length of the variables based on Akaike Information Criterion (AIC). The error terms of the reduced form VAR model have been used to analyse the impulse response of the structural equations of the present study. Sims (1980) states that the reduced form VAR model is purely a forecast model. The estimated error of the reduced form VAR model is presented as a moving average (MA) term that captures how the endogenous variables depend on their lagged residuals of the reduced form VAR model (see 3 and 4). The moving average presentation of the estimated errors of the endogenous variables is presented below.

$$\mathrm{SI}_{\mathrm{it}} = \alpha_{10} + \sum_{\mathrm{j}=1}^{\infty} \mathrm{b}_{11\mathrm{j}} \varepsilon_{1\mathrm{it}-\mathrm{j}} + \sum_{\mathrm{j}=1}^{\infty} \mathrm{b}_{12\mathrm{j}} \in_{2\mathrm{it}-\mathrm{j}} + \sum_{\mathrm{j}=1}^{\infty} \mathrm{b}_{13\mathrm{j}} \in_{3\mathrm{it}-\mathrm{j}} + \sum_{\mathrm{j}=1}^{\infty} \mathrm{b}_{14\mathrm{j}} \varepsilon_{4\mathrm{it}-\mathrm{j}} + \sum_{\mathrm{j}=1}^{\infty} \mathrm{b}_{15\mathrm{j}} \varepsilon_{5\mathrm{it}-\mathrm{j}} + \mu_{1\mathrm{it}} \tag{3}$$

$$\begin{aligned} \mathrm{SI}_{\mathrm{it}} = \alpha_{10} &+ \sum_{\mathrm{j}=1}^{\infty} \mathrm{b}_{11\mathrm{j}} \varepsilon_{1\mathrm{it}-\mathrm{j}} + \sum_{\mathrm{j}=1}^{\infty} \mathrm{b}_{12\mathrm{j}} \in_{2\mathrm{it}-\mathrm{j}} + \sum_{\mathrm{j}=1}^{\infty} \mathrm{b}_{13\mathrm{j}} \in_{3\mathrm{it}-\mathrm{j}} + \sum_{\mathrm{j}=1}^{\infty} \mathrm{b}_{14\mathrm{j}} \varepsilon_{4\mathrm{it}-\mathrm{j}} \\ &+ \sum_{\mathrm{j}=1}^{\infty} \mathrm{b}_{15\mathrm{j}} \varepsilon_{5\mathrm{it}-\mathrm{j}} + \sum_{\mathrm{j}=1}^{\infty} \mathrm{b}_{16\mathrm{j}} \varepsilon_{6\mathrm{it}-\mathrm{j}} + \sum_{\mathrm{j}=1}^{\infty} \mathrm{b}_{17\mathrm{j}} \varepsilon_{7\mathrm{it}-\mathrm{j}} + + \mu_{1\mathrm{it}} \end{aligned} \tag{4}$$

These residuals anticipated correlating, and the estimated coefficients of Eqs. 3 and 4 must be appropriately interpreted. This is because of endogeneity. To counter endogeneity, the residuals must be orthogonalised by multiplying the Cholesky decomposition of the covariance matrix of the residuals. These orthogonalised residuals are measured as random shocks. The moving average representation of the orthogonalised random residuals is called impulse response functions (IRF). It captures the response of each variable included in the model out of one Cholesky standard deviation shock received from each variable of the system. The orthogonalisation of Eqs. 3 and 4 are presented below in Eqs. 5 and 6.

$$\mathrm{SI}_{\mathrm{it}} = \mathrm{A}_{10} + \sum_{\mathrm{j}=1}^{\infty} \mathrm{B}_{11\mathrm{j}} \mathrm{e}_{1\mathrm{it}-\mathrm{j}} + \sum_{\mathrm{j}=1}^{\infty} \mathrm{B}_{12\mathrm{j}} \mathrm{e}_{2\mathrm{it}-\mathrm{j}} + \sum_{\mathrm{j}=1}^{\infty} \mathrm{B}_{13\mathrm{j}} \mathrm{e}_{3\mathrm{it}-\mathrm{j}} + \sum_{\mathrm{j}=1}^{\infty} \mathrm{B}_{14\mathrm{j}} \mathrm{e}_{4\mathrm{it}-\mathrm{j}} + \sum_{\mathrm{j}=1}^{\infty} \mathrm{B}_{15\mathrm{j}} \mathrm{e}_{5\mathrm{it}-\mathrm{j}} + \vartheta_{1\mathrm{it}} \tag{5}$$

$$SI_{it} = A_{10} + \sum_{j=1}^{\infty} B_{11j} e_{1it-j} + \sum_{j=1}^{\infty} B_{12j} e_{2it-j} + \sum_{j=1}^{\infty} B_{13j} e_{3it-j} + \sum_{j=1}^{\infty} B_{14j} e_{4it-j} + \sum_{j=1}^{\infty} B_{15j} e_{5it-j} + \sum_{j=1}^{\infty} B_{16j} e_{6it-j} + \sum_{j=1}^{\infty} B_{17j} e_{7it-j} + +\vartheta_{1it} \quad (6)$$

5 Empirical Analysis

5.1 Pre-estimation Test

Before estimating the response of stock price due to one standard deviation shock (SD) to a system of internal and external macroeconomic shocks using panel impulse response functions (IRF), we first check the stability condition of the estimated panel VAR. The estimated statistics and the eigenvalues measure the overall stability of the panel VAR model are presented in Tables 1 and 2. Since the estimated eigenvalues remain within the unit circle, it confirms stable estimates of panel VAR to ensure its robustness (see Tables 1 and 2). We have used the stability test as a pre-estimation diagnostic test for Panel VAR models measuring the impact of internal and external macroeconomic shocks on the stock returns of BRIC countries.

5.2 Analysing Response of the Equity Market Due to Shocks in Macroeconomic Indicators

The response to Cholesky One SD innovations to stock price with ± 2.5 SE, i.e., 95% confidence interval, is presented in Figs. 1 and 2 for internal and external macroeconomic variables, respectively. The impulse response function of Eqs. 3 and 4

Table 1 Stability Test of Panel VAR model measuring impact of internal macroeconomic shocks on stock returns of BRIC countries

Eigen values	Absolute Eigen values	
0.970	0.970	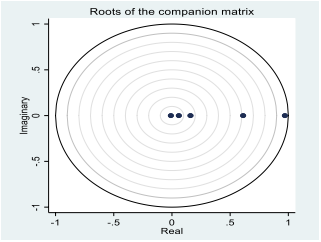
0.601	0.601	
0.159	0.159	
0.058	0.058	
-0.0093	0.0093	

Table 2 Stability Test of Panel VAR model measuring impact of external macroeconomic shocks on stock returns of BRIC countries

Eigen values	Absolute Eigen values
0.977	0.977
0.901	0.901
-0.258	− 0.258
-0.119	− 0.119
0.172	0.172
0.066	0.066

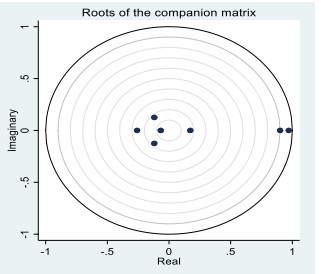

Response of Stock index due to 1 S.D shock in Exchange Rate

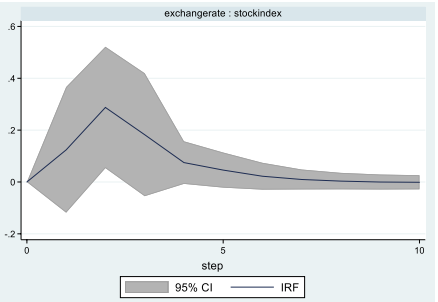

Response of Stock index due to 1 S.D shock in Consumer Price Index (CPI)

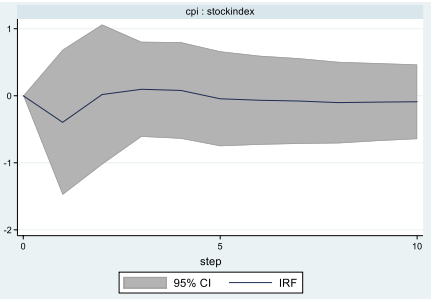

Response of Stock index due to 1 S.D shock in Index of Industrial Production (IIP)

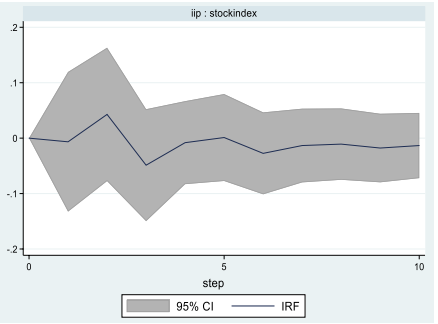

Response of Stock index due to 1 S.D shock in Net Foreign Portfolio *(FPINET)*

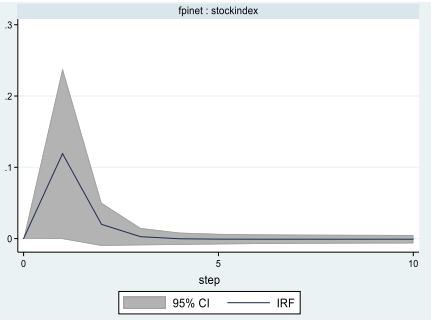

Fig. 1 Graphs analysing impact of internal macroeconomic variable on stock market return of BRICS countries as a system

Response of Stock index due to 1 S.D shock in S & P 500 index *(SPX)*

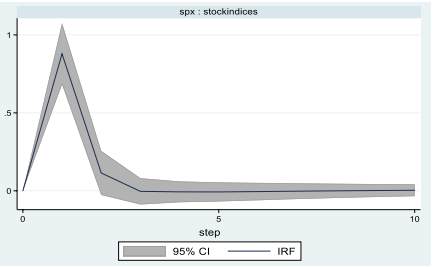

Response of Stock index due to 1 S.D shock in Crude Oil Price

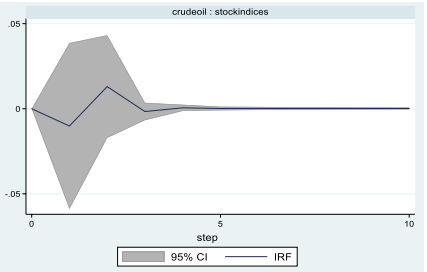

Response of Stock index due to 1 S.D shock in Global Economic Policy (GEPUI)

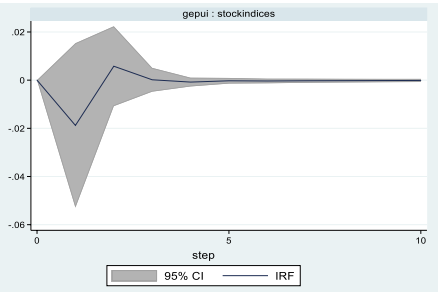

Response of Stock index due to 1 S.D shock in SENTIX global Index (SENTIX)

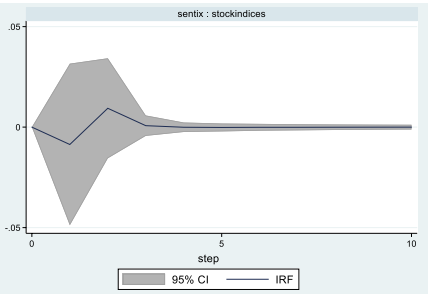

Response of Stock index due to 1 S.D shock in Global Financial Stress Index (GFSI)

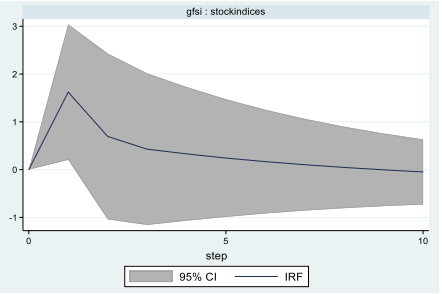

Response of Stock index due to 1 S.D shock in FED Rate (FEDRATE)

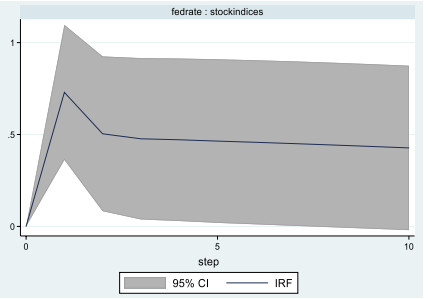

Fig. 2 Graphs analysing impact of external macroeconomic variable on stock market return of BRICS countries as a system

is estimated from Eqs. 1 and 2. Figure 1 shows that the stock price responds positively due to one SD shock to the exchange rate, which takes almost four periods to neutralise. In the case of CPI and FPINET, the immediate response of stock indices is negative, but it starts correcting positively, and its impacts neutralise quickly. The shock of inflation and net foreign portfolio to market returns gets normalised after one period.

On the contrary, the stock markets of BRICS are relatively more volatile due to shocks in the overall economy represented by the index of industrial production. Stock indices oscillate, and the impact of IIP shock can be realised 5–6 periods ahead of index returns of BRICS countries. Among the internal macroeconomic factors, shocks of exchange rate and FPINET remains active for 1–2 periods and are then neutralised. However, the stock market remains sensitive to inflation and economic growth. The wider confidence interval of CPI and IIP is clear evidence that even the shocks look dying out, but the market remains sensitive due to high estimated standard error.

Similarly, for external macroeconomic variables, stock markets respond positively due to shocks in SPX, GFSI, and Fed rate, and the market dilutes the shocks within 2 to 3 periods. Relatively, the response is substantially high due to shock in SPX and Fed Rate. However, stock markets experience volatility and oscillate up to 2–3 periods due to shocks in (CO) crude oil price, GEPUI, and SENTIX. Interestingly, we have noticed that the stock market response due to shocks to SPX, CO, GEPUI, and SENTIX neutralised after 4–5 periods ahead. However, markets remain sensitive respective to GFSI and Fed Rates. Even though the market response dies out within two periods, markets remain sensitive over a long period, evidenced by the high standard error. Moreover, the market remains sensitive to domestic inflation and economic performance among the internal macroeconomic factors and concerning GFSI and Fed Rate among external macroeconomic factors.

5.3 Panel Granger Causality

Although estimates of the panel vector auto-regression model may explain the multivariate relationships among the system of equations, the panel Granger causality Wald tests capture Granger non-causality by expressing each random variable as a function of its lag values and lag values of other variables in the system. Hence the present study estimates Granger causality Wald tests as a post-estimation test to capture the multivariate Granger causality among the system of variables that's stock market returns of the BRICS countries.

5.4 Analysis of Panel Granger Causality

The results for our model, where internal and external macroeconomic variables are independent variables and stock markets are the dependent variables, are presented in Table 3. The Granger causality estimates for the null hypothesis that macroeconomic variable (both from internal and external categories) does not cause stock index are shown in the second and third column of Table 3. Among internal macroeconomic variables, the null hypothesis of an excluded variable does not Granger cause the stock market is rejected at the 5% and 10% significance in the case of the exchange rate, FPINET, and for all variables together. However, among four internal macroeconomic variables, there is not enough evidence against the null hypothesis in the case of CPI and IIP. Similarly, in the case of 6 external macroeconomic variables, the null hypothesis is rejected for SPX, GFSI, and Fed Rate, implying a flow

Table 3 Panel Granger-causality Wald tests

Internal macroeconomic indicators		External macroeconomic indicators	
Excluded variable	*Chi*^{2}	*Excluded variable*	*Chi*^{2}
Exchange rate	3.762**	SPX	86.31***
CPI	0.141	CRUDE OIL	0.185
IIP	0.009	GEPUI	1.197
FPINET	3.537**	SENTIX	0.014
ALL	4.576***	GFSI	5.38***
		FEDRATE	16.21***
		ALL	18.93***

H_0: Excluded variable does not Granger-cause Stock Index

of significant causality to the stock market. The rest of the variables, like Crude Oil, GEPUI, and SENTIX, exhibit strong causality alone to the stock market. However, these macroeconomic indicators significantly influence the stock market as a group of variables.

6 Conclusion

This study examines the dynamic responses of equity returns of BRICS economies due to shocks in internal and international macroeconomic variables. Unlike other studies (Aloui et al., 2011; Bhuyan et al., 2016; Brogaard & Detzel, 2015; Pal & Mittal, 2011; Panda & Thiripalraju, 2020; Patra & Panda, 2021; Rahman et al., 2009), the present study assumes all five economies of BRICS as one economic unit and attempts to measure the response of BRICS equity market returns due to country-specific shocks specific to BRICS countries as well as international macroeconomic shocks which are external to these economies. This makes the study unique of its kind. The study finds that market returns are positively related to exchange rates and respond positively due to news shocks to the exchange rates of these economies. Similarly, markets tend to react negatively to consumer price inflation and changes in foreign portfolio investment, but the impact remains for a short period. However, the equity market is very sensitive to economic growth, as represented by the IIP of BRICS economics. Except for economic growth, the shocks of the rest of the system's variables to the equity market remain for a relatively shorter period. However, a wider confidence interval of these variables gives us a clue that the market will remain sensitive to these indicators, and a small shock to these variables makes the market reactive irrespective of its intensity. Moreover, as a group of variables, these macroeconomic indicators impact stock markets significantly.

The study's empirical findings have significant implications for international investors regarding their portfolio diversification and managing international asset management. Market participants can identify the critical macroeconomic indicators internal and external to the system as systematic risk factors while risk profiling

their portfolio. This has significant implications for constructing and optimising a portfolio regarding the BRICS economy. Policymakers such as central banks may also use the study's findings for market regulation.

The paper has an exciting feature for future research to study the transmission of systemic risk shocks to equity markets and their volatility. It can also be an early warning indicator to measure crisis and its contagion effects. We can also study the impact of macroeconomic news shocks on derivatives markets and their price discovery mechanism.

References

Abugri, B. A. (2008). The empirical relationship between macroeconomic volatility and stock returns: Evidence from Latin American markets. *International Review of Financial Analysis, 17*(2), 396–410.

Aloui, R., Aïssa, M. S. B., & Nguyen, D. K. (2011). Global financial crisis, extreme interdependences, and contagion effects: The role of economic structure? *Journal of Banking & Finance, 35*(1), 130–141.

Bhattacharya, B., & Mukherjee, J. (2006). Indian stock price movements and the macroeconomic context–A time-series analysis. *Journal of International Business and Economics, 5*(1), 167–181.

Bhuyan, R., Robbani, M. G., Talukdar, B., & Jain, A. (2016). Information transmission and dynamics of stock price movements: An empirical analysis of BRICS and US stock markets. *International Review of Economics & Finance, 46*, 180–195.

Brogaard, J., & Detzel, A. (2015). The asset-pricing implications of government economic policy uncertainty. *Management Science, 61*(1), 3–18.

Chen, N. F., Roll, R., & Ross, S. A. (1986). Economic forces and the stock market. *Journal of Business, 59*(3), 383–403.

Dickinson, D. G. (2000). Stock market integration and macroeconomic fundamentals: An empirical analysis, 1980–1995. *Applied Financial Economics, 10*(3), 261–276.

Errunza, V., & Hogan, K. (1998). Macroeconomic determinants of European stock market volatility. *European Financial Management, 4*(3), 361–377.

Fama, E. F. (1981). Stock returns, real activity, inflation, and money. *The American Economic Review, 71*(4), 545–565.

Funke, N., & Matsuda, A. (2002). SttL Working Paper.

Garcia, V. F., & Liu, L. (1999). Macroeconomic determinants of stock market development. *Journal of Applied Economics, 2*(1), 29–59.

Gay, R. D., Jr. (2008). Effect of macroeconomic variables on stock market returns for four emerging economies: A vector regression model for Brazil, Russia, India, and China. *International Business Economics Research Journal, 7*(3), 1–8.

Lubys, J., & Panda, P. (2021). US and EU unconventional monetary policy spillover on BRICS financial markets: An event study. *Empirica, 48*(2), 353–371.

Maysami, R. C., Howe, L. C., & Hamzah, M. A. (2004). Relationship between macroeconomic variables and stock market indices: cointegration evidence from stock exchange of Singapore's All-S sector indices. *Journal Pengurusan, 24*, 47–77.

Mohapatra, S. P., & Panda, B. (2012). Macroeconomic factors (other than the FIIs) affecting the Sensex: An empirical analysis. *Indian Journal of Finance, 6*(11), 35–43.

Mookerjee, R., & Yu, Q. (1997). Macroeconomic variables and stock prices in a small open economy: The case of Singapore. *Pacific-Basin Finance Journal, 5*(3), 377–388.

Mukherjee, T. K., & Naka, A. (1995). Dynamic relations between macroeconomic variables and the Japanese stock market: An application of a vector error correction model. *Journal of Financial Research, 18*(2), 223–237.

Naik, P., & Puja, P. (2012). *The impact of macroeconomic fundamentals on stock prices revisited: An Evidence from Indian Data*. University Library of Munich.

Pal, K., & Mittal, R. (2011). Impact of macroeconomic indicators on Indian capital markets. *The Journal of Risk Finance, 12*(2), 84–97.

Panda, P., & Deo, M. (2014a). Asymmetric cross-market volatility spillovers: Evidence from Indian equity and foreign exchange markets. *Decision, 41*(3), 261–270.

Panda, P., & Deo, M. (2014b). Asymmetric and volatility spillover between stock market and foreign exchange market: Indian experience. *IUP Journal of Applied Finance, 20*(4), 69.

Panda, P., & Thiripalraju, M. (2020). Stock markets, macroeconomics and financial structure of BRICS countries and USA. *Prajnan, 49*(2), 123–159.

Patra, S., & Panda, P. (2021). Spillovers and financial integration in emerging markets: Analysis of BRICS economies within a VAR-BEKK framework. *International Journal of Finance & Economics, 26*(1), 493–514.

Rahman, A. A., Sidek, N. Z. M., & Tafri, F. H. (2009). Macroeconomic determinants of Malaysian stock market. *African Journal of Business Management, 3*(3), 95–106.

Ratanapakorn, O., & Sharma, S. C. (2007). Dynamic analysis between the US stock returns and the macroeconomic variables. *Applied Financial Economics, 17*(5), 369–377.

Sharma, G. D., & Mahendru, M. (2010). Impact of macro-economic variables on stock prices in India. *Global Journal of Management and Business Research, 10*(7), 19–26.

Sims, C. A. (1980). Macroeconomics and reality. *Econometrica, 48*(1), 1–48.

Sireesha, P. (2013). Effect of select macro-economic variables on stock returns in India. *International Journal of Marketing, Financial Services & Management Research, 2*(6), 197–209.

24. Kavanagh, A. J., Kosch, M. J., Honary, F., Senior, A., Marple, S. R., Woodfield, E. E., McCrea, I. W., The statistical dependence of auroral absorption on geomagnetic and solar wind parameters. Ann. Geophys. 22, 877-887, 2004.

25. Kavanagh, A. J., Honary, F., Donovan, E. F., Ulich, T., Denton, M. H. Key features of >30 keV electron precipitation during high speed solar wind streams: A superposed epoch analysis. J. Geophys. Res. 117, A00L09, doi:10.1029/2011JA017320, 2012.

26. Kellerman, A. C., Makarevich, R. A. The response of auroral absorption to substorm onset: Superposed epoch and propagation analyses. J. Geophys. Res. 116, A05312, doi:10.1029/2010JA015972, 2011.

27. Kikuchi, T., Yamagishi, H., Lester, M. Drift of auroral absorption due to the magnetospheric convection observed with the scanning narrow beam riometer during SUNDIAL. Ann. Geophys. 8, 431-440, 1990.

28. Korotova, G. I., Sibeck, D. G., Rosenberg, T. J., Russell, C. T., Friis-Christensen, E. High-latitude ionospheric transient events in a global context. J. Geophys. Res. 102(A8), 17499–17508, doi:10.1029/97JA00939, 1997.

29. Kullen, A., Karlsson, T. On the relation between solar wind, pseudobreakups, and substorms. J. Geophys. Res. 109, A12218, doi:10.1029/2004JA010488, 2004.

30. Liou, K., Newell, P. T., Shue, J.-H., Meng, C.-I., Miyashita, Y., Kojima, H., Matsumoto, H. "Compression aurora": Particle precipitation driven by long-duration high solar wind ram pressure. J. Geophys. Res. 112, A11216, doi:10.1029/2007JA012443, 2007.

31. Meredith, N. P., Horne, R. B., Lam, M. M., Denton, M. H., Borovsky, J. E., Green, J. C.. Energetic electron precipitation during high-speed solar wind stream driven storms. J. Geophys. Res. 116, A05223, doi:10.1029/2010JA016293, 2011.

32. Newell, P. T., Meng, C.-I. Mapping the dayside ionosphere to the magnetosphere according to particle precipitation characteristics. Geophys. Res. Lett. 19 (6), 609-612, 1992.

33. Nielsen, E. Dynamics and spatial scale of auroral absorption spikes associated with the substorm expansion phase. J. Geophys. Res. 85, 2092–2098, 1980.

34. Partamies, N., Juusola, L., Tanskanen, E., and Kauristie, K. Statistical properties of substorms during different storm and solar cycle phases. Ann. Geophys. 31, 349-358, doi:10.5194/angeo-31-349-2013, 2013.

35. Ranta, H., Ranta, A., Collis, P. N., Hargreaves, J. K. Development of the auroral absorption substorm: Studies of pre-onset phase and sharp onset using an extensive riometer network. Planet. Space Sci. 29, 1287-1313, 1981.

36. Singh, A. K., Sinha, A. K., Rawat, R., Jayashree, B., Pathan, B. M., Dhar, A. A broad climatology of very high latitude substorms. Adv. Space Res. 50, 1512-1523, doi:10.1016/j.asr.2012.07.034, 2012.